Optical Frequency Doubling

Benjamin Lovitz

Department of Physics and Astronomy, Bates College, Lewiston, ME 04240

Optical Frequency Doubling

A Senior Thesis

Presented to the Department of Physics and Astronomy

Bates College

in partial fulfillment of the requirements for the

Degree of Bachelor of Arts

by

Benjamin Lovitz

Lewiston, Maine

April 6, 2015

Contents

List of Tables iii

List of Figures iv

Acknowledgments v

Introduction vi
Outline vi

Chapter 1. Gaussian Beam Optics 1
1. The Paraxial Wave Equation 1
2. Gaussian Beam Solution to the Paraxial Wave Equation 2

Chapter 2. Michelson Interferometer 8
1. Theory 8
2. Practice 10

Chapter 3. Nonlinear Optics 12
1. The Nonlinear Electron Oscillator 12
2. Perturbative Solution to the Nonlinear Oscillator Equation 14
3. Nonlinear Polarization 16
4. Wave Propagation in Nonlinear Media 17
5. Optical Second-Harmonic Generation 20

Chapter 4. SHG Optimization 21
1. Critical Phase Matching 21
2. Walk-Off Angle 25
3. Focused Gaussian Beam SHG Optimization 29
4. Resonant Enhancement Cavity 30
5. Cavity Stabilization 31

Appendix 35
Intensity of Monochomatic Plane Waves 35

Bibliography 37

List of Tables

1 Gaussian Beam Solution to the Paraxial Wave Equation 7

1 Relevant values for optimal second harmonic generation with given input beam characteristics. 33

2 Crystal Specifications. 34

List of Figures

1.1 Geometric aid to deriving the phase delay of a spherical wave. 4

2.1 Michelson interferometer with moveable mirror [**1**] 8
2.2 Predicted intensity output for $\delta L = 16.6$cm and λ near 780nm. 10
2.3 Actual intensity output of recombined beam as internal laser piezo is driven by a triangle wave. 11

3.1 Noncentrosymmetric potential energy function [**2**]. 13

4.1 A light beam with two orthogonal field components traversing a negative uniaxial crystal. The ordinary ray experiences a refractive index $n_o(\omega)$ and the extraordinary ray experiences a refractive index $n_e(\omega, \theta)$. 22
4.2 Interatomic dipole moments and Brewster's angle [**3**]. 25
4.3 Type I o-o-e critical phase matching in a negative uniaxial crystal cut at the phase matching angle θ_p and with faces cut at Brewster's angle θ_B [**4**]. 25
4.4 Ellipsoidal wavelets of e-wave in a negative uniaxial crystal [**3**]. 26
4.5 Orientations of the $\vec{E}, \vec{S}, \vec{D}$, and $\vec{k}$ vectors for ordinary and extraordinary wavelets [**3**]. 27
4.6 Walk-off angle. 27
4.7 Bowtie cavity for resonant enhancement of the input fundamental wave [**5**]. 30
4.8 Hänsch-Couillaud cavity locking scheme [**5**]. 31
4.9 Plot of error signal (4.46) as function of detuning from resonance in Hänsch-Couillaud locking scheme. 32
4.10 Hänsch-Couillaud locking scheme used to lock the laser frequency to be resonant with a cavity [**6**]. 33

Acknowledgments

"We've been here before. We're going in circles!" Samwise Gamgee

Thank you Cookie and Mica for your love and support; part of me rests with you. Thank you Mom and Dad for everything that cannot be put into words. Thank you David for your wisdom to teach me right from wrong and for keeping me true to myself. Thank you wonderful people from home, Parker first, 106 Central (R.I.P), Carriage house, and Asian studies lounge for your invaluable distraction and support. Thank you Dr. Nathan Lundblad for your time, insight and advice.

Introduction

This thesis introduces the topic of *optical frequency doubling*, which is the physical process in which a high-intensity optical field produces a nonlinear polarization in a medium, and in turn gives rise to an electromagnetic wave with twice the frequency of the applied field. Quantum mechanically, pairs of photons with the same frequency are effectively "combined" to form new photons with twice the energy (and thus twice the frequency and half the wavelength) of the initial photons.

Nonlinear polarization effects only arise when the optical field is on the order of the interatomic electric fields of the medium (usually 10^5 to 10^8 V/m). Such high intensity optical fields were not available until the invention of the laser in 1960, so the phenomenon was not demonstrated until 1961 by Peter Franken, A. E. Hill, C. W. Peters, and G. Weinreich at the University of Michigan, Ann Arbor [**7**]. The formulation of second harmonic generation was first described by N. Bloembergen and P. S. Pershan at Harvard in 1962 [**8**].

In practice, the optical field is sent through a nonlinear crystal for second harmonic generation. Several crystals (BBO, LBO, KTP, BiBO, $KNbO_3$, PPLN) are used for second harmonic generation at different frequencies. We have obtained a barium borate (BBO) crystal to frequency double 800nm laser light. In future work the crystal will be placed in a resonant cavity that is locked to the fundamental frequency to increase the fundamental pump power sent through the crystal. The second harmonic power generated increases quadratically with the pump power.

Since its discovery, optical frequency doubling has found many experimental applications. Our motivation derives from a theoretical proposal set forth by Masuda et. al (2014) to use the doubled light in a BEC apparatus for faster adiabatic loading of the condensate into an optical lattice [**9**]. Black box frequency doublers are available commercially at prices ranging from twenty to fourty thousand dollars, but building one is much less costly.

Outline

- Theoretical review and derivation of Gaussian beam optics.
- Review of studies of the Michelson interferometer, which was built to characterize a diode laser system and understand the relevant piezoelectric control mechanisms for use in the resonant cavity.
- Derivation of second harmonic generation beginning from the nonlinear electron oscillator model.
- For efficient second harmonic generation the index of refraction must be identical for the fundamental and second harmonic waves. We discuss critical phase matching, which accomplishes this by sending the fundamental beam into a birefringent doubling crystal at a special angle of incidence called the phase matching angle. Another method called quasi-phase matching uses precise temperature control of a periodically poled doubling crystal.

- Discussion of the Boyd-Kleinman theory of focused Gaussian beam SHG optimization.
- Overview of the optical resonance cavity and locking scheme.

CHAPTER 1

Gaussian Beam Optics

In this chapter we derive Gaussian beam optics, which are indispensable to characterizing any laser system (including the frequency doubling scheme). The Gaussian beam equations are solutions to the paraxial wave equation, which assumes that the laser beam propagation is nearly paraxial. We assume a nearly paraxial cylindrically symmetric wave propagating in the $+\hat{k}$ direction. Our derivation follows closely that given in [**10**].

1. The Paraxial Wave Equation

In this section we derive the paraxial wave equation. We begin with the wave equation for an electric field in a vacuum:

$$\nabla^2 E(\vec{r},t) - \frac{1}{c^2}\frac{\partial^2}{\partial t^2}E(\vec{r},t) = 0. \tag{1.1}$$

We examine only the scalar wave equation instead of the full vector form. This analysis will therefore not take into account polarization effects. Assume a solution of the form

$$E(\vec{r},t) = \mathscr{E}(\vec{r})e^{-i\omega t} \tag{1.2}$$

which is a single frequency (monochromatic) electric field. We now substitute (1.2) into (1.1), use the wavenumber $k = \frac{2\pi}{\lambda} = \frac{2\pi}{2\pi c/\omega} = \frac{\omega}{c}$, and divide by $e^{-i\omega t}$:

$$\nabla^2 \mathscr{E}(\vec{r}) + k^2 \mathscr{E}(\vec{r}) = 0. \tag{1.3}$$

This is called the *Helmholtz equation* for $\mathscr{E}(\vec{r})$. We assume the beam propagates along the z-axis. For an ideal plane wave propagating along the z-axis we would have $\frac{\partial^2 \mathscr{E}(\vec{r})}{\partial x^2} = \frac{\partial^2 \mathscr{E}(\vec{r})}{\partial y^2} = 0$. This would produce a solution to (1.3) given by

$$\mathscr{E}(\vec{r}) = Ae^{ikz}. \tag{1.4}$$

Thus, for a non-plane wave propagating along the z-axis we try a solution with an e^{ikz} term along with a correction term $\mathscr{E}_0(\vec{r})$:

$$\mathscr{E}(\vec{r}) = \mathscr{E}_0(\vec{r})e^{ikz}. \tag{1.5}$$

Now we assume that the wave propagation is nearly paraxial. Namely, we assume that within a distance of the order of a wavelength in the $\hat{k}$ direction, changes in $\mathscr{E}_0$ and $\partial\mathscr{E}_0/\partial z$ are negligible:

$$\lambda\left|\frac{\partial \mathscr{E}_0}{\partial z}\right| \ll \left|\mathscr{E}_0\right| \tag{1.6}$$

$$\lambda\left|\frac{\partial^2 \mathscr{E}_0}{\partial^2 z}\right| \ll \left|\frac{\partial \mathscr{E}_0}{\partial z}\right| \tag{1.7}$$

and since $k = 2\pi/\lambda$,

$$\left|\frac{\partial \mathscr{E}_0}{\partial z}\right| \ll k\left|\mathscr{E}_0\right| \tag{1.8}$$

$$\left|\frac{\partial^2 \mathscr{E}_0}{\partial^2 z}\right| \ll k\left|\frac{\partial \mathscr{E}_0}{\partial z}\right|. \tag{1.9}$$

We know (1.5) must satisfy the Helmholtz equation (1.3):

$$\Big(\frac{\partial^2}{\partial x^2} + \frac{\partial^2}{\partial y^2} + \frac{\partial^2}{\partial z^2}\Big)\mathscr{E}_0(\vec{r})e^{ikz} + k^2\mathscr{E}_0(\vec{r})e^{ikz} = 0. \tag{1.10}$$

Using the product rule we have

$$\frac{\partial^2}{\partial z^2}\mathscr{E}_0(\vec{r})e^{ikz} = \Big(\frac{\partial^2 \mathscr{E}_0}{\partial z^2} + 2ik\frac{\partial \mathscr{E}_0}{\partial z} - k^2\mathscr{E}_0\Big)e^{ikz} \tag{1.11}$$

$$\approx \Big(2ik\frac{\partial \mathscr{E}_0}{\partial z} - k^2\mathscr{E}_0\Big)e^{ikz} \tag{1.12}$$

under the approximation given by (1.9). Combining (1.12) and (1.10) gives

$$\Big(\frac{\partial^2}{\partial x^2} + \frac{\partial^2}{\partial y^2} + 2ik\frac{\partial}{\partial z}\Big)\mathscr{E}_0(\vec{r}) \cong 0. \tag{1.13}$$

Substituting the *transverse Laplacian* defined as $\nabla_T^2 \equiv \frac{\partial^2}{\partial x^2} + \frac{\partial^2}{\partial y^2}$ we arrive at the *paraxial wave equation* for the correction term $\mathscr{E}_0(\vec{r})$:

$$\nabla_T^2\mathscr{E}_0 + 2ik\frac{\partial \mathscr{E}_0}{\partial z} = 0. \tag{1.14}$$

2. Gaussian Beam Solution to the Paraxial Wave Equation

Laser beams are frequently observed to have a Gaussian beam intensity profile

$$I(x, y, z) \sim |\mathscr{E}_0(\vec{r})|^2 e^{-2(x^2+y^2)/w^2} \tag{1.15}$$

where w is called the spot size, and is the lateral distance from the z axis at which the intensity is $1/e^2$ of its on-axis value. We construct a solution to (1.14) which will produce this intensity profile. Namely,

$$\mathscr{E}_0(\vec{r}) = Ae^{ik(x^2+y^2)/2q(z)}e^{ip(z)} \tag{1.16}$$

where A is a constant and $q(z)$ and $p(z)$ are to be determined.

We now determine $q(z)$ and $p(z)$. To this end, we first compute the requisite derivatives:

$$\frac{\partial \mathscr{E}_0}{\partial z} = iA\left(\frac{dp}{dz} - \frac{k}{2}(x^2+y^2)\frac{1}{q^2}\frac{dq}{dz}\right)e^{ik(x^2+y^2)/2q(z)}e^{ip(z)} \tag{1.17}$$

and

$$\nabla_T^2\mathscr{E}_0 = A\left(\frac{2ik}{q} - \frac{k^2}{q^2}(x^2+y^2)\right)e^{ik(x^2+y^2)/2q(z)}e^{ip(z)}. \tag{1.18}$$

Substituting these expressions into (1.14) gives

$$\nabla_T^2\mathscr{E}_0 + 2ik\frac{\partial \mathscr{E}_0}{\partial z} = A\left(\frac{k^2}{q^2}(x^2+y^2)\left(\frac{dq}{dz} - 1\right) - 2k\left(\frac{dp}{dz} - \frac{i}{q}\right)\right)e^{ik(x^2+y^2)/2q(z)}e^{ip(z)} = 0. \tag{1.19}$$

Thus, (1.16) will be a solution to (1.14) if

$$\frac{dq}{dz} = 1 \tag{1.20}$$

and

$$\frac{dp}{dz} = \frac{i}{q}. \tag{1.21}$$

Solving (1.20) gives

$$q(z) = q_0 + z \tag{1.22}$$

where $q_0 = q(0)$. Substituting (1.22) into (1.21) gives the differential equation

$$\frac{dp}{dz} = \frac{i}{q_0 + z}. \tag{1.23}$$

If we assume $p(0) = 0$ we can integrate this expression explicitly:

$$p(z) = i \ln \frac{q_0 + z}{q_0}. \tag{1.24}$$

Now we define $1/q$ as

$$\frac{1}{q(z)} = \frac{1}{R(z)} + \frac{i\lambda}{\pi w^2(z)}. \tag{1.25}$$

We arrive at the imaginary term in (1.25) from the observation that as $R \to \infty$, $1/q \to \frac{i\lambda}{\pi w^2(z)}$, and using this expression for $1/q$ in (1.16) produces the desired Gaussian intensity profile (1.15). The real part $1/R$ can be thought of as an arbitrary function of z. However, a close analogy can be drawn between R and the radius of curvature of a spherical wave [**11**]. Substituting (1.25) and $r^2 = x^2 + y^2$ into (1.16) the q-dependent term becomes

$$\exp\left(\frac{ikr^2}{2q(z)}\right) = \exp\left[\left(\frac{ikr^2}{2}\right)\left(\frac{1}{R(z)}\right) - \left(\frac{kr^2}{2}\right)\left(\frac{\lambda}{\pi w^2(z)}\right)\right]. \tag{1.26}$$

The $1/R$ term in (1.26) is imaginary, and thus accounts for a phase shift. We now show this phase shift is identical to the phase delay of a spherical wave with radius of curvature R. As shown in Figure 1.1a, we designate $\phi(r)$ to be the phase delay (in radians) relative to the plane defined by a fixed value of z at some radius r from the z-axis.
We now derive an expression for $\phi(r)$. Using the geometry of Figure 1.1b we have

$$R = R\cos\theta + \phi(r)\frac{\lambda}{2\pi}. \tag{1.27}$$

In the paraxial approximation $r \ll R$. Thus, $\theta \ll 1$, so $\cos\theta \cong 1 - \theta^2/2$ and $\theta \cong \sin\theta = r/R$. Thus,

$$R \cong R - \frac{(r/R)^2}{2} + \phi(r)\frac{\lambda}{2\pi}. \tag{1.28}$$

Rearranging terms we find

$$\phi(r) \cong \frac{\pi r^2}{\lambda R} = \frac{kr^2}{2R} \tag{1.29}$$

which is identical to the imaginary term in (1.26). This equivalence implies that for a fixed value of z the Gaussian beam wavefront is approximately spherical with radius of curvature R.

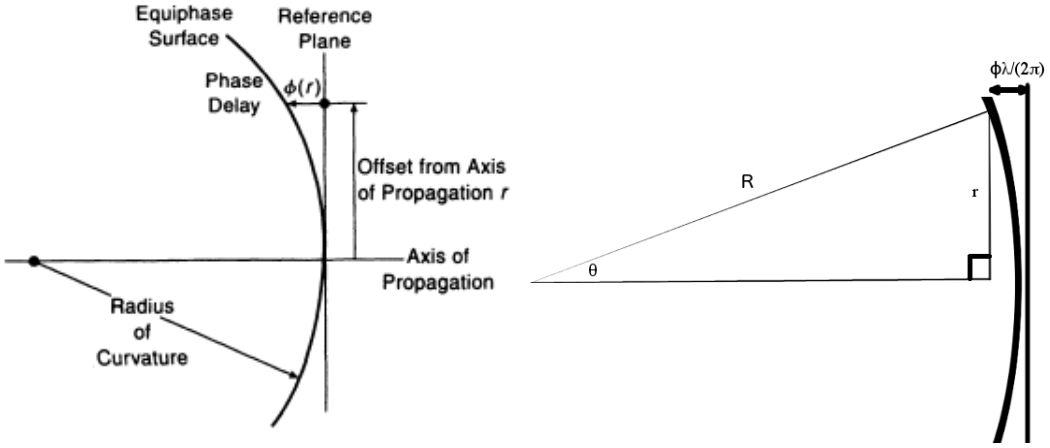

(A) Phase delay $\phi(r)$ in a spherical wave at a distance r from the axis of propagation [**11**].

(B) Spherical wave geometry

FIGURE 1.1. Geometric aid to deriving the phase delay of a spherical wave.

Now we use (1.24) in (1.25) to get

$$\begin{aligned} e^{ip(z)} &= \exp\left[-\ln\frac{q_0+z}{q_0}\right] \\ &= \frac{q_0}{q_0+z} \\ &= \frac{1}{1+z/q_0} \\ &= \frac{1}{1+z/R_0+i\lambda z/\pi w_0^2} \end{aligned} \tag{1.30}$$

where R_0 and w_0 are the values of R and w at $z=0$.

If R_0 and w_0 are known, then (1.22) and (1.25) give $R(z)$ and $w(z)$ for all values of z. We assume our laser converges to some minimum spot size. We call this minimum spot size the *beam waist* w_0. Since the designation $z=0$ is arbitrary, we choose it to be the point on the z-axis at which the beam converges to w_0. Since the beam is neither converging nor diverging at $z=0$ the wave is approximately planar at this point. This implies R_0 is infinitely large, so

$$R_0 = \infty \tag{1.31}$$

and

$$\frac{1}{q_0} = \frac{i\lambda}{\pi w_0^2}. \tag{1.32}$$

Thus,

$$\begin{aligned} \frac{1}{q(z)} = \frac{1}{q_0+z} &= \frac{1}{\frac{i\lambda}{\pi w_0^2}+z} \\ &= \frac{z-\frac{i\lambda}{\pi w_0^2}}{z^2+\frac{\lambda^2}{\pi^2 w_0^4}} = \frac{1}{R(z)}+\frac{i\lambda}{\pi w^2(z)}. \end{aligned} \tag{1.33}$$

Equating the real and imaginary parts gives

$$R(z) = z + \frac{z_0^2}{z} \tag{1.34}$$

$$w(z) = w_0\sqrt{1 + z^2/z_0^2} \tag{1.35}$$

where we define z_0 to be

$$z_0 = \frac{\pi w_0^2}{\lambda}. \tag{1.36}$$

This parameter is known as the *Rayleigh range*.

Equations (1.31) and (1.36) allow us to write (1.30) as

$$e^{ip(z)} = \frac{1}{1 + iz/z_0}. \tag{1.37}$$

We define

$$\mu(z) = \tan^{-1}(z/z_0) \tag{1.38}$$

so that

$$e^{ip(z)} = \frac{1}{\sqrt{1 + z^2/z_0^2}} e^{-i\mu(z)}. \tag{1.39}$$

Using this equation and (1.26) in (1.15) we have

$$\mathscr{E}_0(\vec{r}) = \frac{Ae^{-i\mu(z)}}{\sqrt{1 + z^2/z_0^2}} e^{ikr^2/2R(z)} e^{-r^2/w^2(z)}. \tag{1.40}$$

Multiplying by e^{ikz} gives the complete expression for the spatially dependent component of the electric field $\mathscr{E}(\vec{r})$.

Note that (1.35) implies

$$w(z_0) = w_0\sqrt{2}. \tag{1.41}$$

Thus, the Rayleigh range z_0 is a measure of the length of the region where the beam waist is within a $\sqrt{2}$ multiple of w_0. Note that $w(z_0)$ varies as w_0, and from (1.36) z_0 varies as w_0^2. Since the former relation is linear and the latter quadratic we know a smaller beam waist w_0 will produce a greater rate of increase with z of the spot size $w(z)$. Thus, focusing the beam to small w_0 has the cost of large beam divergence. Note we cannot make w_0 too small or else the beam divergence will be too great for the paraxial approximation (1.8) and (1.9) to hold.

We define the angular divergence θ of the Gaussian beam to be the angle between $\omega(z)$ (the distance from the z-axis at which the intensity drops to $1/e^2$ of its on-axis value) and the z axis. When $z \gg z_0$ the angular divergence is given by

$$\theta \approx \tan\theta = \frac{w(z)}{z} \approx \frac{w_0}{z_0} = \frac{\lambda}{\pi w_0}, \qquad z \gg z_0 \tag{1.42}$$

Thus, the beam waist w_0 must be large compared with the wavelength λ for the angular divergence to be small and the paraxial approximation to apply.

With (1.40) in hand, it is straightforward to derive the intensity of the field averaged over an optical period:

$$I(r, z) = \frac{c\epsilon_0}{2}|\mathscr{E}(r, z)|^2 = \frac{(c\epsilon_0/2)|A|^2}{1 + z^2/z_0^2} e^{-2r^2/w^2(z)} \tag{1.43}$$

Thus, the rate at which energy crosses any plane defined by a constant z value is

$$\int_0^{2\pi}\int_0^{\infty} I(r,z) r dr d\theta = \frac{(c\epsilon_0/2)|A|^2}{1+z^2/z_0^2}\int_0^{2\pi}\int_0^{\infty} e^{-2r^2/w^2(z)} r dr d\theta$$

$$= \frac{c\epsilon_0}{4}|A|^2(\pi w_0^2) \tag{1.44}$$

Note that this expression is independent of z, which is consistent with the conservation of energy.

It is useful to consider the limit $z \gg z_0$, as it arises frequently in laser systems. In this limit $1/(1+z^2/z_0^2) = z_0^2/(z_0^2+z^2) \approx z_0^2/z^2$ and the beam intensity becomes

$$I(r,z) = (c\epsilon_0/2)|A|^2 \frac{z_0^2}{z^2} e^{-2r^2/w^2(z)}, \qquad z \gg z_0. \tag{1.45}$$

When $z \gg z_0$ we have

$$\sqrt{1+z^2/z_0^2} = z/z_0\sqrt{1+z_0^2/z^2} \approx z/z_0 \tag{1.46}$$

so that

$$w(z) = w_0\sqrt{1+z^2/z_0^2} \approx \frac{w_0 z}{z_0} = \frac{\lambda z}{\pi w_0}, \qquad z \gg z_0 \tag{1.47}$$

which is a linear function of the distance z from the beam waist. Additionally, note that when $z \gg z_0$, $\mu(z) = \tan^{-1}(z/z_0) \approx \pi/2$. Thus,

$$\mathscr{E}(\vec{r}) \approx (c\epsilon_0/2)|A|^2 \frac{z_0}{z} e^{i(kz-\pi/2)} e^{ikr^2/2R(z)} e^{-r^2/w^2(z)}, \qquad z \gg z_0 \tag{1.48}$$

We can reduce this further by noting when $z \gg z_0$, (1.34) becomes

$$R \approx z, \qquad z >> z_0 \tag{1.49}$$

so that

$$\mathscr{E}(\vec{r}) \approx -i(c\epsilon_0/2)|A|^2 z_0 \left[\frac{1}{z} e^{ikz} e^{ikr^2/2z}\right] e^{-r^2/w^2(z)}, \qquad z \gg z_0 \tag{1.50}$$

The bracketed portion is identical to the field from a spherical wave with center of curvature located at the beam waist [**10**]. In fact, (1.50) takes exactly the same form as a spherical wave for points close enough to the z-axis that

$$e^{-r^2/w^2(z)} \approx 1. \tag{1.51}$$

It is interesting to note that the field strength (1.40) for a given value of z is determined only by the amplitude constant A, the wavelength λ, and the beam waist w_0 (the Rayleigh range z_0 is determined from these quantities). Incredibly, these parameters alone fully characterize any nearly paraxial Gaussian beam.

(1.52a)	$E(\vec{r}) = \mathscr{E}_0(\vec{r})e^{ikz}e^{-iwt}$	(electric field)
(1.52b)	$\mathscr{E}_0(\vec{r}) = \dfrac{Ae^{-i\mu(z)}}{\sqrt{1+z^2/z_0^2}}e^{ikr^2/2R(z)}e^{-r^2/w^2(z)}$	
(1.52c)	$\mu(z) = \tan^{-1}(z/z_0)$	
(1.52d)	$I(r,z) = \dfrac{c\epsilon_0}{2}\lvert\mathscr{E}(r,z)\rvert^2 = \dfrac{(c\epsilon_0/2)\lvert A\rvert^2}{1+z^2/z_0^2}e^{-2r^2/w^2(z)}$	(intensity)
(1.52e)	$w(z) = w_0\sqrt{1+\dfrac{z^2}{z_0^2}}$	(spot size)
(1.52f)	$R(z) = z + \dfrac{z_0^2}{z}$	(radius of curvature)
(1.52g)	$z_0 = \pi w_0^2/\lambda$	(Rayleigh range)
(1.52h)		

TABLE 1. Gaussian Beam Solution to the Paraxial Wave Equation

CHAPTER 2

Michelson Interferometer

Before studying optical second harmonic generation directly we built a Michelson interferometer to characterize a diode laser system and develop an understanding of the relevant piezoelectric control mechanisms for use in the resonant cavity. This involved piezoelectric control of the mirrors and laser frequency. In this chapter we give a theoretical treatment of the Michelson interferometer, followed by a brief account of our confirmation of this theory in the lab.

1. Theory

When two beams of equal frequency interfere they create a circular interference pattern of bright and dark fringes on whatever surface they are incident upon. The Michelson interferometer produces this phenomenon by using a beam splitter to divide monochromatic light into two beams which reflect off of mirrors placed at different distances from the beam splitter before recombining in the splitter and creating an interference pattern on a nearby photodiode.

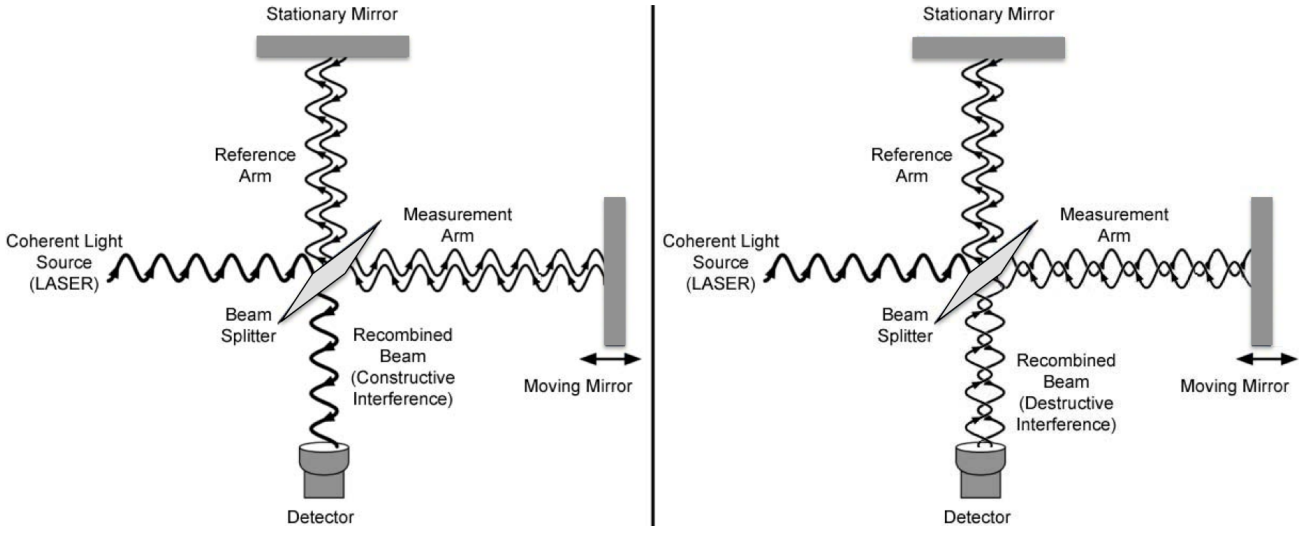

FIGURE 2.1. Michelson interferometer with moveable mirror [**1**]

As depicted in Figure 2.1 when the difference in distance δL traveled between the two beams is an integer number of wavelngths (left) the two interfere constructively when recombined. When $\delta L = (n + 1/2)\lambda$ (right) the beams interfere destructively. We can switch between constructive and destructive interference either by changing the optical path length difference δL or by changing the frequency of the input beam.

We assume the beam splitter splits the input beam into two beams which are monochromatic plane waves of equal amplitude traveling in a vacuum in the z-direction with phases ϕ_1 and ϕ_2:

$$E_1(z,t) = \frac{1}{2}\big[\mathscr{E}_0 e^{i\phi_1} e^{i\omega t} + c.c.\big] \tag{2.1}$$

$$E_2(z,t) = \frac{1}{2}\big[\mathscr{E}_0 e^{i\phi_2} e^{i\omega t} + c.c.\big]. \tag{2.2}$$

Since the two beams originate from the same input beam their fields are identical besides the phase difference. When these two beams are superimposed the resulting field is

$$E_f(z,t) = E_1(z,t) + E_2(z,t) \tag{2.3}$$

$$= \frac{1}{2}\mathscr{E}_0\big[e^{i\phi_1} + e^{i\phi_2}\big]e^{i\omega t} + c.c.. \tag{2.4}$$

The intensity of a monochromatic wave is given by (see Appendix)

$$I = \frac{1}{2}\sqrt{\frac{\epsilon_0}{\mu}}|E_0(z)|^2 \tag{2.5}$$

where $E_0(z)$ is the complex amplitude of the wave. Applying this expression to the input waves $E_1(z)$ and $E_2(z)$ gives

$$I_1 = \frac{1}{2}\sqrt{\frac{\epsilon_0}{\mu}}|\mathscr{E}_0 e^{i\phi_1}|^2 \tag{2.6}$$

and

$$I_2 = \frac{1}{2}\sqrt{\frac{\epsilon_0}{\mu}}|\mathscr{E}_0 e^{i\phi_2}|^2. \tag{2.7}$$

Both expressions simplify to

$$I_1 = I_2 = \frac{1}{2}\sqrt{\frac{\epsilon_0}{\mu}}|\mathscr{E}_0|^2. \tag{2.8}$$

Applying (2.5) to the optical field of the recombined beam (2.4) gives

$$I_f = \frac{1}{2}\sqrt{\frac{\epsilon_0}{\mu}}\left|\mathscr{E}_0\big(e^{i\phi_1} + e^{i\phi_2}\big)\right|^2 \tag{2.9}$$

$$= \frac{1}{2}\sqrt{\frac{\epsilon_0}{\mu}}\left(|\mathscr{E}_0 e^{i\phi_1}|^2 + |\mathscr{E}_0 e^{i\phi_2}|^2 + \mathscr{E}_0^2\big[e^{i(\phi_1-\phi_2)} + e^{i(\phi_2-\phi_1)}\big]\right) \tag{2.10}$$

$$= \frac{1}{2}\sqrt{\frac{\epsilon_0}{\mu}}\left(|\mathscr{E}_0 e^{i\phi_1}|^2 + |\mathscr{E}_0 e^{i\phi_2}|^2 + 2\mathscr{E}_0^2\cos(\phi_2-\phi_1)\big]\right) \tag{2.11}$$

$$= 2I_1(1+\cos\phi) \tag{2.12}$$

where $\phi = \phi_2 - \phi_1$. Now we assume the first wave has traveled a distance z and the second has traveled a distance $z + \delta L$ where δL is the path length difference between the two beams. This implies

$$\phi_1 = -kz \tag{2.13}$$

$$\phi_2 = -k(z+\delta L) \tag{2.14}$$

so

$$\phi = \phi_2 - \phi_1 = k\delta L = \frac{2\pi\delta L}{\lambda} \tag{2.15}$$

which implies

$$I_f = 2I_1\left[1 + \cos\left(\frac{2\pi\delta L}{\lambda}\right)\right]. \tag{2.16}$$

In sum, we have found the intensity I_f that results from the interference of two plane waves of equal intensity I_0 and wavelength λ which have traveled a difference in optical path length δL.

2. Practice

We confirmed (2.16) both by changing the wavelength λ and the optical path length difference δL. We changed δL with a piezoelectric transducer (PZT) placed on one of the mirrors of the interferometer. The piezo varied significantly only with very high voltage input (50-100V), which is greater than our function generator can produce. With no source of reproducible input voltage we could only confirm the theory qualitatively by changing δL using a hand-adjustable voltage generator and observing the corresponding intensity of the recombined beam on the oscilloscope.

The wavelength λ was changed using a piezo placed on one of the intracavity mirrors. Changing the intracavity resonator length changes the wavelength of light which resonates with the cavity and is output by the laser. We used a 780nm diode laser. The difference in distance between the beam splitter and each mirror of the interferometer was 8.3cm, which corresponds to an optical path length difference $\delta L = 16.6$cm. The piezo changes the wavelength of the laser as a function of voltage input, which we found to be $(7.9 \pm .1) \times 10^{-4}$nm/Volt.

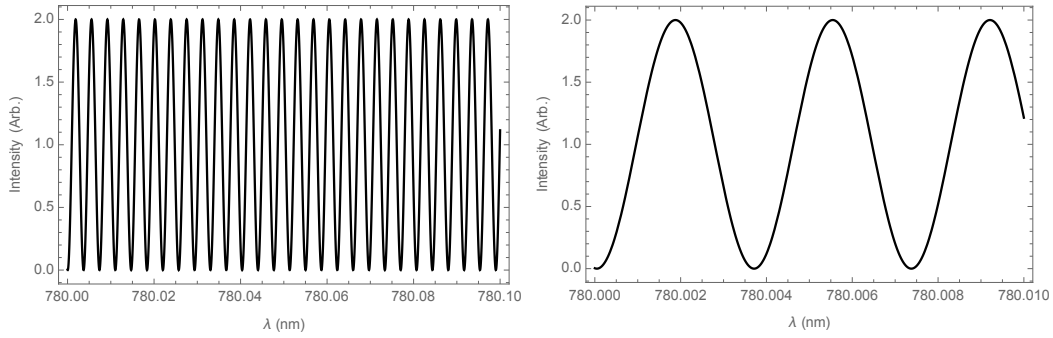

(A) (B)

FIGURE 2.2. Predicted intensity output for $\delta L = 16.6$cm and λ near 780nm.

Above are plots of (2.16) over different ranges of λ. According to Figure 2.2b the two beams should go from destructive interference to constructive interference over a wavelength change of $\sim .002$nm.

We tested this prediction by driving the piezo with a triangle wave produced by a function generator and measuring the intensity of the recombined beam with a photodiode linked to an oscilloscope. Two examples of the plots produced in the oscilloscope are given in Figures 2.3a and 2.3b. The "cusps" where the sinusoidal pattern is broken represent where the triangle wave reaches maximum or minimum amplitude and begins to change the wavelength in the opposite direction. The amplitude of the triangle wave driving the piezo for Figure 2.3a is clearly greater than that of Figure 2.3b because the former traverses 1.5 periods of constructive to destructive interference between each cusp and the latter traverses only half a period.

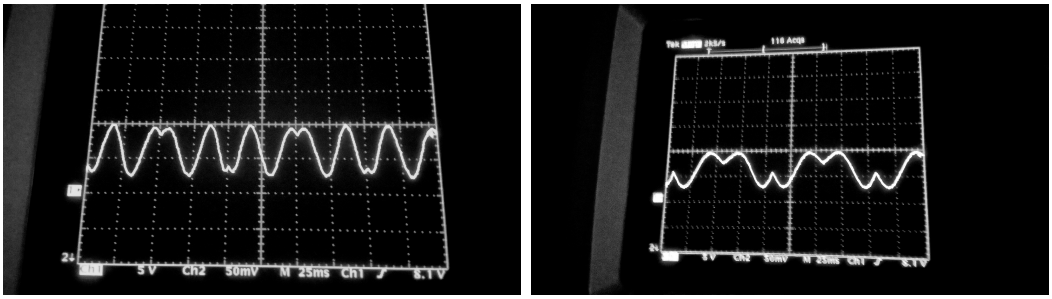

(A) (B)

FIGURE 2.3. Actual intensity output of recombined beam as internal laser piezo is driven by a triangle wave.

Figure 2.3a gives the output intensity when the laser piezo is driven by a triangle wave of frequency $f = 10\text{Hz}$ and peak-to-peak amplitude $V_{p2p} = 8.7\text{V}$. The intensity traverses 1.5 periods (3 bright-dark transitions) in $(32 \pm 2)\text{ms}$, so one bright-dark transition corresponds to a wavelength change of

$$\begin{aligned}\Delta\lambda =& \Delta\text{V} \times 7.86 \times 10^{-4}\text{nm/Volt} \\ =& \left[\frac{1}{3}\left(32 \times 10^{-3}\text{s}\right) \times \frac{8.7\text{V}}{1/20\text{s}}\right] \times 7.9 \times 10^{-4}\text{nm/Volt} \\ =& 0.0015\text{nm}\end{aligned}$$

which is within uncertainty of our predicted value $\sim .002\text{nm}$.

Figure 2.3b gives the output intensity from an input triangle wave of frequency $f = 10\text{Hz}$ and peak-to-peak amplitude $V_{p2p} = 5.7\text{V}$. The intensity traverses one bright-dark transition in $(25 \pm 2)\text{ms}$, which corresponds to a wavelength change of

$$\begin{aligned}\Delta\lambda =& \Delta\text{V} \times 7.86 \times 10^{-4}\text{nm/Volt} \\ =& \left[\left(25 \times 10^{-3}\text{s}\right) \times \frac{5.7\text{V}}{1/20\text{s}}\right] \times 7.9 \times 10^{-4}\text{nm/Volt} \\ =& 0.0022\text{nm}\end{aligned}$$

for one bright-dark transition, which also matches the predicted value quite well.

CHAPTER 3

Nonlinear Optics

Nonlinear optics is the branch of optics which describes the behavior of light in *nonlinear media*, that is, media in which the polarization $\vec{P}$ responds nonlinearly to the optical field. As we will see, this phenomenon gives rise to the useful property of optical second harmonic frequency generation. Nonlinear optics arise when the intensity of the applied optical field is comparable to the interatomic electric fields of the nonlinear medium (usually 10^5 to 10^8 V/m), so the phenomenon was not discovered until the invention of the laser in 1960. Just as a mechanical oscillator can be overdriven into a nonlinear response through the application of large forces, so too can a high intensity laser produce a nonlinear polarization of the optical medium. For this analysis we make frequent reference to the treatments presented in [**10**], [**2**], [**12**], and [**13**].

1. The Nonlinear Electron Oscillator

In this section we derive the nonlinear effects produced when an electron on a spring is overdriven by an oscillating electric field. This derivation follows closely that given in [**10**]. For an electron on an ideal spring placed in an electric field $E(t)$ the equation of motion is

$$m\frac{d^2x}{dt^2} = -eE(t) - m\omega_0^2 x \tag{3.1}$$

where $x(t)$ is the displacement of the electron from its equilibrium position. With an ideal spring the restoring force in (3.1) is associated with a potential energy

$$U(x) = \frac{1}{2}m\omega_0^2 x^2 \tag{3.2}$$

but with a real spring we cannot make this assumption. For a real spring the effective potential energy (whatever form it takes) can be expanded as a Taylor series about the equilibrium position $x = 0$:

$$U(x) = U(0) + x\left(\frac{dU}{dx}\right)_{x=0} + \frac{1}{2!}x^2\left(\frac{d^2U}{dx^2}\right)_{x=0} + \frac{1}{3!}x^3\left(\frac{d^3U}{dx^3}\right)_{x=0} + \ldots. \tag{3.3}$$

The first term $U(0)$ may be neglected because it is constant and thus does not produce any force (F=-dU/dx). Additionally, at $x = 0$ the potential energy is a minimum, which implies

$$\left(\frac{dU}{dx}\right)_{x=0} = 0. \tag{3.4}$$

With these observations we may write

$$U(x) = \frac{1}{2!}x^2\left(\frac{d^2U}{dx^2}\right)_{x=0} + \frac{1}{3!}x^3\left(\frac{d^3U}{dx^3}\right)_{x=0} + \ldots. \tag{3.5}$$

Note if odd powers of x are present in the expansion then the potential energy (and thus the restoring force) cannot be centrosymmetric. This means the nonlinear medium lacks inversion symmetry.

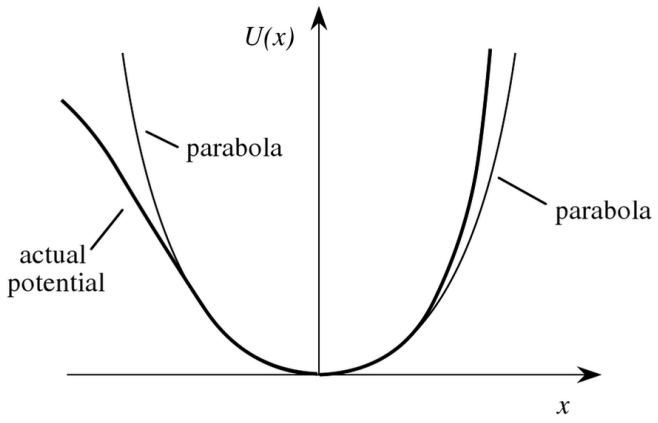

FIGURE 3.1. Noncentrosymmetric potential energy function [**2**].

Since the force is restorative, $x = 0$ must be a stable equilibrium. Thus,

$$\left(\frac{d^2U}{dx^2}\right)_{x=0} > 0 \tag{3.6}$$

which allows us to define

$$m\omega_0^2 \equiv \left(\frac{d^2U}{dx^2}\right)_{x=0}. \tag{3.7}$$

Interestingly, it is the curvature of the effective potential energy which determines the oscillator frequency ω_0. For simplicity, we introduce new variables A and B defined as

$$A \equiv \frac{1}{3!}\left(\frac{d^3U}{dx^3}\right)_{x=0} \tag{3.8}$$

$$B \equiv \frac{1}{4!}\left(\frac{d^4U}{dx^4}\right)_{x=0} \tag{3.9}$$

and implicitly define C, D and so on to be the higher order Taylor series coefficients. These definitions simplify the Taylor series to

$$U(x) = \frac{1}{2}m\omega_0^2x^2 + Ax^3 + Bx^4 + \dots. \tag{3.10}$$

Since $A, B, \dots$ do not depend on x, we can determine the restoring force by taking the spatial derivative of (3.10):

$$F = -\frac{dU}{dx} = -m\omega_0^2x - 3Ax^2 - 4Bx^3 + \dots \tag{3.11}$$

which implies the equation of motion is

$$\ddot{x} + w_0^2x + \frac{3A}{m}x^2 + \frac{4B}{m}x^3 + \dots = -\frac{e}{m}E(t). \tag{3.12}$$

In the event of an ideal spring with a perfectly elastic restoring force, $A = B = \dots = 0$ and we recover the simple harmonic oscillator equation (3.1). As we will see, it is precisely the nonlinear terms in (3.12) that produce the nonlinear optical effects which give rise to second harmonic generation.

In reality, atoms are governed by quantum mechanics and not by the Newtonian mechanics of restorative forces. However, to a large extent the quantum-mechanical theory of nonlinear

optical susceptibility merely provides a method of calculating $A, B, \ldots$ from first principles, without changing the nature of (3.10). Quantum mechanics also allows each atom to possess many energy eigenvalues and thus more than one resonance frequency ω_0. However, this analysis gives a quite adequate description of nonlinear optics when all of the optical frequencies are well below the lowest electronic resonance frequency of the medium. Under this assumption we can treat nonlinear optics quite satisfactorily with this classical analysis.

2. Perturbative Solution to the Nonlinear Oscillator Equation

Based on the success of the linear oscillator model, we expect the nonlinear terms to be quite small. For the first nonlinear term to be significant we must have

$$m\omega_0^2 x \sim 3Ax^2 \tag{3.13}$$

or

$$x \sim \frac{m\omega_0^2}{3A}. \tag{3.14}$$

If $3A/m \ll \omega_0^2$ then the displacement x must be quite large for the first nonlinear term to be appreciable. This is consistent with experimental observations that nonlinear matter-field interactions do not arise until high intensity electromagnetic fields are applied.

For the following analysis we assume that the quadratic term is the only significant nonlinearity. We also assume a damping force of the form $-m\sigma\dot{x}$. The constant σ is known as the conductivity of the medium. Under these assumptions the nonlinear electron oscillator equation becomes

$$\ddot{x} + \sigma\dot{x} + w_0^2 x + ax^2 = -\frac{e}{m}E(t) \tag{3.15}$$

where $a = 3A/m$. We assume a simple oscillating electric field given by

$$E(t) = \frac{1}{2}(E_0 e^{-i\omega t} + c.c) \tag{3.16}$$

There is no known general solution to (3.15) for an applied electric field of the form (3.16). However, if we assume a is small in the sense described above we may treat it as a perturbation of the linear oscillator equation.

We proceed with a method analogous to that of Rayleigh-Schrödinger perturbation theory in quantum mechanics. We replace $E(t)$ by $\lambda E(t)$, where λ is the perturbation constant which varies continuously between zero and one. At the end of the calculation we set λ equal to one. Equation (3.15) becomes

$$\ddot{x} + \sigma\dot{x} + w_0^2 x + ax^2 = -\lambda\frac{e}{m}E(t). \tag{3.17}$$

We now seek a solution to (3.17) in the form of a power series expansion of λ, namely

$$x = \lambda x^{(1)} + \lambda^2 x^{(2)} + \lambda^3 x^{(3)} + \ldots. \tag{3.18}$$

In order for (3.18) to be a solution to (3.17) for arbitrary λ, coefficients of each power of λ must maintain the equality in (3.17). Equating the λ, λ^2, and λ^3 coefficients respectively gives

$$\ddot{x}^{(1)} + \sigma\dot{x}^{(1)} + \omega_0^2 x^{(1)} = -\frac{e}{m}E(t) \tag{3.19}$$

$$\ddot{x}^{(2)} + \sigma\dot{x}^{(2)} + \omega_0^2 x^{(2)} + a[x^{(1)}]^2 = 0 \tag{3.20}$$

$$\ddot{x}^{(3)} + \sigma\dot{x}^{(3)} + \omega_0^2 x^{(2)} + 2ax^{(1)}x^{(2)} = 0. \tag{3.21}$$

As expected, the lowest-order contribution $x^{(1)}$ is governed by the linear oscillator model (3.19). The steady-state solution to (3.19) is

$$x^{(1)}(t) = \frac{1}{2}\big[a^{(1)}(\omega)e^{-i\omega t} + c.c.\big], \tag{3.22}$$

where the amplitude $a^{(1)}(\omega)$ is given by

$$a^{(1)}(\omega) = -\frac{e}{m}\frac{E_0}{D(\omega)} \tag{3.23}$$

and we have introduced the complex denominator

$$D(\omega) = w_0^2 - \omega^2 - i\omega\sigma. \tag{3.24}$$

The homogeneous solution to (3.19) is given by

$$x^{(1)}_{\text{hom}}(t) = [A\cos\omega_0' t + B\sin\omega_0' t]e^{-\frac{\sigma}{2}t} \tag{3.25}$$

where

$$\omega_0' = (\omega_0^2 - \sigma^2/4)^{1/2} \approx \omega_0. \tag{3.26}$$

If the oscillator has realistic relaxation then

$$t \gg 1/\sigma \tag{3.27}$$

which implies $e^{-\frac{\sigma}{2}t} \approx 0$. Thus, we can neglect the homogeneous solution because it is a short-lived contribution to the general solution which quickly damps to zero.

Now we square the expression for $x^{(1)}(t)$ and substitute into (3.20). The square of $x^{(1)}(t)$ contains the frequencies $\pm 2\omega$ and 0. To determine the nonlinear response at frequency 2ω we solve the equation

$$\ddot{x}^{(2)} + \sigma\dot{x}^{(2)} + \omega_0^2 x^{(2)} = \frac{-a(eE_0/m)^2 e^{-2i\omega t}}{D^2(\omega)}. \tag{3.28}$$

For the same reasons as above, we can ignore the homogenous solution. Based on the observation above we seek steady-state solutions to (3.28) of the form

$$x_1^{(2)}(t) = \frac{1}{2}(a^{(2)}(2\omega)e^{-2i\omega t} + c.c.) \tag{3.29}$$

and

$$x_2^{(2)}(t) = a^{(2)}(0). \tag{3.30}$$

Substitution of (3.29) and (3.30) into (3.28) gives

$$a^{(2)}(2\omega) = \frac{-a(e/m)^2 E_0^2}{2D(2\omega)D^2(\omega)}. \tag{3.31}$$

and

$$a^{(2)}(0) = \frac{-a(e/m)^2 E_0 E_0^*}{2D(0)D(\omega)D(-\omega)} \tag{3.32}$$

where we have made use of the definition (3.24) of the denominator function $D(\omega)$. Combining the linear and nonlinear results gives

$$x(t) \approx x^{(1)}(t) + x_1^{(2)}(t) + x_2^{(2)}(t) \tag{3.33}$$

$$= \frac{1}{2}(a^{(1)}(\omega)e^{-i\omega t} + c.c.) + \frac{1}{2}(a^{(2)}(2\omega)e^{-2i\omega t} + c.c.) + a^{(2)}(0). \tag{3.34}$$

In sum, we have characterized the linear and first-order nonlinear response of a damped harmonic oscillator. We have seen that the motion of the electron has a component oscillating at twice the frequency of the applied optical field.

3. Nonlinear Polarization

In this section we show that the $\pm 2\omega$ component of the oscillating electron motion produces a nonlinear component of the medium's resulting polarization, which in turn produces electromagnetic radiation at frequency 2ω. The following treatment of nonlinear dielectrics follows closely the analyses presented in [**2**], [**14**], and [**3**].

We assume the polarization density $\vec{P}$ and the applied electric field $\vec{E}$ point in the same direction, so we can proceed with scalar quantities. Nonlinear dielectrics are characterized by a nonlinear relation between P and E. Even in nonlinear dielectrics, external optical fields are typically much smaller than the interatomic fields of the medium and the standard linear relation

$$P^{(1)} = \epsilon_0 \chi^{(1)} E \tag{3.35}$$

is a good approximation. Even when focused laser light is used, the nonlinear effects are quite weak. Thus, for small E the relationship is approximately linear, and becomes only slightly nonlinear as E increases. This allows us to expand the function relating P to E as a Taylor series about $E = 0$:

$$P = a_1 E + \frac{1}{2} a_2 E^2 + \frac{1}{6} a_3 E^3 + \dots . \tag{3.36}$$

The coefficients a_1, a_2 and a_3 are the first, second, and third derivatives of P with respect to E at $E = 0$. For (3.36) to be consistant with (3.35) we observe $a_1 = \epsilon_0 \chi^{(1)}$. The second term represents a quadratic or second-order nonlinearity, the third a third-order noninearity, and so on. Renaming terms so that $\chi^{(2)} = a_2/2$, $\chi^{(3)} = a_3/6$, etc. gives

$$P = \epsilon_0 \chi^{(1)} E + \chi^{(2)} E^2 + \chi^{(3)} E^3 + \dots . \tag{3.37}$$

The coefficients $\chi^{(j)}$ with $j > 1$ are called the nonlinear susceptibilities of the medium.

The polarization density P is defined as the electric dipole moment per unit volume. Approximating the atomic structure of the medium as a collection of electric dipoles with displacement $\vec{d}(t) = ex(t)$ then P can also be expressed as

$$P = Nex(t) \tag{3.38}$$

where N is the number of molecules per unit volume and x is the electron distance from equilibrium.

In solving (3.15), our expression (3.34) for $x(t)$ contains two nonlinear components: $x_1^{(2)}(t)$, which oscillates at 2ω, and $x_2^{(2)}(t)$, which is a DC offset term of zero frequency. The former is proportional to E_0^2 and the latter is proportional to $E_0 E_0^*$. Therefore, both are proportional to the (real) amplitude squared of E_0, which we call $\mathscr{E}_0$. Since E_0 is arbitrary, then $\mathscr{E}_0$ is also arbitrary, and equating (3.37) and (3.38) implies that coefficients corresponding to each power of $\mathscr{E}_0$ must also be equal.

By the logic above, since $x_1^{(2)}(t)$ is nonzero and proportional to $\mathscr{E}_0^2$, then the nonlinear susceptibility $\chi^{(2)}$ must be nonzero. Thus, the first nonlinear term of the polarization density expansion, given by

$$P^{(2)} = \chi^{(2)} E^2 \tag{3.39}$$

is nonzero. In reality, $\chi^{(1)}$ and $\chi^{(2)}$ are tensors which depend on the frequency and direction of the optical field. This complicates the analysis significantly, and is outside the scope of this work. We will take these susceptibilities to be empirical parameters. For a more complete treatment see [**2**], which derives the first and second order susceptibility corrections at each frequency by equating each component of the electron motion approximation (3.34) in (3.38) with the corresponding component of the other polarization density expression (3.37).

In sum, we have found that the presence of $\mathscr{E}_0^2$ proportional terms in our approximation of $x(t)$ implies the existence of an E^2 dependent term in the expansion of P. Substituting our expression (3.16) for $E(t)$ into (3.39) gives

$$\begin{aligned} P^{(2)} =& \chi^{(2)} E^2 \\ =& \chi^{(2)} \left[\frac{1}{2} (E_0 e^{-i\omega t} + E_0^* e^{i\omega t}) \right]^2 \\ =& \chi^{(2)} \frac{1}{4} \left[E_0^2 e^{-i2\omega t} + (E_0^*)^2 e^{i2\omega t} + 2E_0 E_0^* \right]. \end{aligned} \tag{3.40}$$

Thus, the E^2 dependent term in P contains components oscillating at frequencies $\pm 2\omega$ and 0. In [**2**] these components are shown to arise directly from the nonlinear components of $x(t)$ oscillating at frequencies $\pm 2\omega$ and 0. Also presented in [**2**] is the generalization to an applied electric field with two frequency components ω_1 and ω_2, which produce sum $\omega_1 + \omega_2$ and difference $\omega_1 - \omega_2$ components of $x(t)$ and $P^{(2)}$. This treatment will continue to focus solely on the case of second harmonic generation.

4. Wave Propagation in Nonlinear Media

We have just seen that when an optical field oscillating at frequency ω is applied to a nonlinear medium it produces a nonlinear polarization component oscillating at frequency 2ω. In this section we use this polarization in Maxwell's equations to derive expressions for the propagation of the electromagnetic wave through the medium. In the following section these expressions will be used to infer second harmonic generation. This treatment follows closely that given in [**12**].

Maxwell's equations are given by

$$\nabla \times \vec{H} = \vec{J} + \frac{\partial \vec{D}}{\partial t} \tag{3.41}$$

$$\nabla \times \vec{E} = -\mu \frac{\partial \vec{H}}{\partial t} \tag{3.42}$$

and

$$\vec{D} = \epsilon_0 \vec{E} + \vec{P} \tag{3.43}$$

$$\vec{J} = \sigma \vec{E} \tag{3.44}$$

where $\vec{D}$ and $\vec{H}$ are the electric and magnetic displacement vectors, $\vec{E}$ and $\vec{B}$ are the electric and magnetic field vectors, $\vec{P}$ is the polarization, $\vec{J}$ is the current density, and σ is the conductivity. In writing (3.41) and (3.42) we have assumed the nonlinear medium to be nonferromagnetic so that the magnetic dipole moment per unit volume $\vec{M}$ is approximately zero.

We define $\vec{P}_{\text{NL}}$ to be the sum of nonlinear components of $\vec{P}$ so that

$$\vec{P} = \epsilon_0 \chi^{(1)} \vec{E} + \vec{P}_{\text{NL}} \tag{3.45}$$

and (3.41) becomes

$$\nabla \times \vec{H} = \sigma \vec{E} + \epsilon \frac{\partial \vec{E}}{\partial t} + \frac{\partial}{\partial t} \vec{P}_{\mathrm{NL}} \tag{3.46}$$

where the definition $\epsilon \equiv \epsilon_0(1 + \chi^{(1)})$ has been used.

For this analysis we assume that all electric fields involved are infinite transverse plane waves propagating in the z-direction. Since the propagation direction is perpendicular to $\vec{E}$, then clearly $\nabla \cdot \vec{E} = 0$. For Gaussian beams $\nabla \cdot \vec{E}$ is non-zero, but can be shown to be small in comparison to other terms in the expression.

Taking the curl of both sides of (3.42), using (3.46) and the vector identity

$$\nabla \times \nabla \times \vec{E} = \nabla \nabla \cdot \vec{E} - \nabla^2 \vec{E} \tag{3.47}$$

and taking $\nabla \cdot \vec{E} = 0$ gives

$$\nabla^2 \vec{E} = \mu\sigma \frac{\partial \vec{E}}{\partial t} + \mu\epsilon \frac{\partial^2 \vec{E}}{\partial t^2} + \mu \frac{\partial^2}{\partial t^2} \vec{P}_{\mathrm{NL}}. \tag{3.48}$$

We assume $\vec{E}$ and $\vec{P}$ are parallel so we can rewrite (3.48) in scalar notation as

$$\nabla^2 E = \mu\sigma \frac{\partial E}{\partial t} + \mu\epsilon \frac{\partial^2 E}{\partial t^2} + \mu \frac{\partial^2}{\partial t^2} P_{\mathrm{NL}}. \tag{3.49}$$

We have assumed E to be an infinite plane wave propagating in the z-direction:

$$E^{(\omega)}(z,t) = \frac{1}{2}\big[E_1(z) e^{i(\omega t - k_1 z)} + c.c.\big]. \tag{3.50}$$

As the electromagnetic wave propagates through the nonlinear medium we will prove in the next section that it acquires a second harmonic component given by

$$E^{(2\omega)}(z,t) = \frac{1}{2}\big[E_2(z) e^{i(2\omega t - k_2 z)} + c.c.\big] \tag{3.51}$$

which oscillates with frequency 2ω. In fact, it also acquires components at frequencies 3ω, 4ω, and so on, but we are only concerned with the second harmonic for this analysis. Adding both components gives the total electric field

$$E(z,t) = E^{(\omega)}(z,t) + E^{(2\omega)}(z,t). \tag{3.52}$$

Note that each component of this electric field is consistent with (3.16) under proper definition of E_0.

By (3.39), we square the electric field (3.52) to find first nonlinear term $P^{(2)}$ of the nonlinear polarization P_{NL}. Squaring (3.52) we find that $P^{(2)}$ contains components at frequencies 0, ω, 2ω, 3ω and 4ω. We concern ourselves only with the ω and 2ω components, which are given by

$$P_{\mathrm{NL}}^{(2\omega)} = \frac{1}{2} d\big[E_1^2(z) e^{i(2\omega t - 2k_1 z)} + c.c.\big] \tag{3.53}$$

and

$$P_{\mathrm{NL}}^{(\omega)} = \frac{1}{4} d\big[E_2(z) E_1^*(z) e^{i[\omega t - (k_2 - k_1) z]} + c.c.\big] \tag{3.54}$$

where we have used $d = \chi^{(2)}/2$, the standard notation for the first nonlinear coefficient. It should be emphasized that, in general, d depends not only on the medium, but also on the direction of wave propagation through the medium and the frequencies involved.

We split (3.49) into separate equations by frequency dependence. Using our expression (3.54) for $P_{\mathrm{NL}}^{(\omega)}$ the ω term becomes

$$\nabla^2 E^{(\omega)} = \mu\sigma_1 \frac{\partial E^{(\omega)}}{\partial t} + \mu\epsilon_1 \frac{\partial^2 E^{(\omega)}}{\partial t^2} + \mu d \frac{\partial^2}{\partial t^2}\left[\frac{E_2(z)E_1^*(z)}{4} e^{i[\omega t-(k_2-k_1)z]} + c.c.\right]. \tag{3.55}$$

We now obtain an expression for $\nabla^2 E^{(\omega)}$:

$$\begin{aligned} \nabla^2 E^{(\omega)} &= \frac{1}{2}\frac{\partial^2}{\partial z^2}\left[E_1(z)e^{i(\omega t-k_1 z)} + c.c.\right] \\ &\approx -\frac{1}{2}\left[k_1^2 E_1(z) + 2ik_1 \frac{dE_1(z)}{dz}\right] e^{i(\omega t-k_1 z)} + c.c. \end{aligned} \tag{3.56}$$

where we assumed

$$\left|k_1 \frac{dE_1(z)}{dz}\right| \gg \left|\frac{d^2 E_1(z)}{dz^2}\right|. \tag{3.57}$$

This is a reasonable approximation because the nonlinear medium is uniform, so we do not expect drastic fluctuations in the electric field amplitude as the optical field propagates through the medium. This is called the slowly-varying-amplitude approximation, and is discussed further in Section 2.2 of [**2**]. This approximation implies the second spatial derivative of $E_1(z)$ will be much smaller than the first, as stated in (3.57).

The first and second time derivatives of $E^{(\omega)}$ are given by

$$\frac{\partial E^{(\omega)}}{\partial t} = i\omega \frac{E_1(z)}{2} e^{i(\omega t-k_1 z)} + c.c. \tag{3.58}$$

and

$$\frac{\partial^2 E^{(\omega)}}{\partial t^2} = -\omega^2 \frac{E_1(z)}{2} e^{i(\omega t-k_1 z)} + c.c.. \tag{3.59}$$

Evaluating the third term in (3.55) gives

$$\mu d \frac{\partial^2}{\partial t^2}\left[\frac{E_2(z)E_1^*(z)}{4} e^{i(2\omega t-2k_1 z)} + c.c.\right] = -\left[\frac{\omega^2 \mu d}{4} E_2(z)E_1^*(z) e^{i[\omega t-(k_2-k_1)z]} + c.c.\right]. \tag{3.60}$$

Substituting (3.56), (3.58), (3.59) and (3.60) into (3.55), recognizing that $k_1^2 = \omega^2\mu\epsilon_1$ and multiplying all terms by

$$\frac{i}{k_1}\exp(-i\omega t + ik_1 z) \tag{3.61}$$

gives

$$\frac{dE_1}{dz} = -\frac{\sigma_1}{2}\sqrt{\frac{\mu}{\epsilon_1}} E_1 - \frac{i\omega}{4}\sqrt{\frac{\mu}{\epsilon_1}} dE_2 E_1^* e^{-i(k_2-2k_1)z} \tag{3.62}$$

and a nearly identical analysis gives

$$\frac{dE_2}{dz} = -\frac{\sigma_2}{2}\sqrt{\frac{\mu}{\epsilon_2}} E_2 - \frac{i2\omega}{2}\sqrt{\frac{\mu}{\epsilon_2}} dE_1^2 e^{-i(2k_1-k_2)z}. \tag{3.63}$$

These are the equations describing wave propagation in a nonlinear medium. We note that they are coupled to eachother by the nonlinear coefficient d. See [**12**] for a generalization to an electric field consisting of two arbitrary frequencies ω_1 and ω_2 and a sum frequency $\omega_1 + \omega_2$.

5. Optical Second-Harmonic Generation

In this section we use the derived wave equation (3.63) for the second harmonic component of E to determine $E^{(2\omega)}(t)$. For simplicity, we ignore absorption so $\sigma_{1,2} = 0$, which is a good approximation in most optical media. Equation (3.63) becomes

$$\frac{dE_2(z)}{dz} = -i\omega\sqrt{\frac{\mu}{\epsilon_2}}dE_1^2(z)e^{i(\Delta k)z} \tag{3.64}$$

where

$$\Delta k = k_2 - 2k_1 = k^{(2\omega)} - 2k^{(\omega)}. \tag{3.65}$$

To further simplify this analysis, we assume that the depletion of the input wave at ω due to interaction with the medium is negligible. Under these conditions, which apply in most experimental situations, we can take $E_1(z)$ as constant and neglect its z-dependence. Since the input wave has no 2ω component, then $E_2(0) = 0$. Under these assumptions we integrate (3.64) over a crystal of length l to obtain

$$E_2(l) = -i\omega\sqrt{\frac{\mu}{\epsilon_2}}dE_1^2\frac{e^{i\Delta kl} - 1}{i\Delta k}. \tag{3.66}$$

The output intensity is then proportional to

$$E_2(l)E_2^*(l) = \frac{\mu}{\epsilon_0}\frac{\omega^2 d^2}{n_{2\omega}^2}|E_1|^4 l^2\frac{\sin^2(\Delta kl/2)}{(\Delta kl/2)^2} \tag{3.67}$$

where we used $\epsilon_2/\epsilon_0 = n_{2\omega}^2$ with $n_{2\omega}$ the index of refraction of the medium for an applied optical field at 2ω. If we confine the input beam to a cross sectional area A then the power per unit area (intensity) is given by (see Appendix)

$$I_{2\omega} \equiv \frac{P_{2\omega}}{A} = \frac{1}{2}\sqrt{\frac{\epsilon_2}{\mu}}|E_2|^2 \tag{3.68}$$

$$I_{\omega} \equiv \frac{P_{\omega}}{A} = \frac{1}{2}\sqrt{\frac{\epsilon_1}{\mu}}|E_1|^2 \tag{3.69}$$

Combining these expressions with (3.67) we can write

$$\eta_{\text{SHG}} \equiv \frac{P_{2\omega}}{P_{\omega}} = 2\left(\frac{\mu}{\epsilon_0}\right)^{3/2}\frac{\omega^2 d^2 l^2}{n_{\omega}^2 n_{2\omega}}\frac{\sin^2(\Delta kl/2)}{(\Delta kl/2)^2}\frac{P_{\omega}}{A} \tag{3.70}$$

for the conversion efficiency from ω to 2ω. Interestingly, the conversion efficiency is proportional to the intensity P_ω/A of the fundamental beam. An analagous procedure with a focused Gaussian beam input reveals a conversion efficiency identical to (3.70) with A replaced by πw_0^2 under the assumption $z_0 >> l$, where $z_0 = \pi w_0^2 n/\lambda$ is the Rayleigh range of the Gaussian beam.

According to (3.70) the conversion efficiency will surpass 100% for sufficiently large input power, which violates conservation of energy. This error is a direct result of our assumption that $E_1(z)$ is constant with time. Thus, (3.70) only applies when η_{SHG} is small. For a more accurate treatment we would have to consider the depletion of the pump radiation as it is converted to the second harmonic. This would require analyzing in tandem both derived differential equations for the wave propagation (3.62) and (3.63) which couple $E_1(z)$ and $E_2(z)$ through the nonlinear coefficient d. For our setup, η_{SHG} is small enough so that (3.70) holds. For a treatment of second harmonic generation with input depletion see [**10**], [**2**], [**14**], or [**12**].

CHAPTER 4

SHG Optimization

In this chapter we outline the techniques that could be used to optimize the SHG light generated. First we maximize (3.70) to optimize single-pass efficiency. We then introduce the resonant cavity and associated locking scheme which allow the pump beam to pass through the crystal many times and greatly increase the SHG light generated.

1. Critical Phase Matching

The conversion efficiency (3.70), will be maximized when $\Delta k = 0$ or, using (3.65),

$$k^{(2\omega)} = 2k^{(\omega)}, \tag{4.1}$$

which is a direct result of the mathematical relation

$$\lim_{x\to 0} \frac{\sin(x)}{x} = 1. \tag{4.2}$$

As the input field propagates through the medium it continuously generates light at the second harmonic. The second harmonic field propagates with phase velocity $c/n_{2\omega}$, whereas (3.54) dictates the nonlinear polarization source has phase velocity c/n_{ω}. This discrepancy produces a phase difference in the fields given by $\Delta k \neq 0$, which we have shown reduces the output power by a factor of

$$\frac{\sin^2(\Delta k l/2)}{(\Delta k l/2)^2}. \tag{4.3}$$

We can express Δk as a function of the indices of refraction of the medium at ω and 2ω:

$$\Delta k = k^{(2\omega)} - 2k^{(\omega)} = \frac{2\omega}{c}[n_{2\omega} - n_{\omega}] \tag{4.4}$$

where we used the relation $k = \omega n/c$. Thus, we must have

$$n_{2\omega} = n_{\omega} \tag{4.5}$$

for maximum conversion efficiency.

In normally dispersive materials the refractive index increases with ω, which makes (4.5) difficult to achieve. One method uses the birefringence of uniaxial crystals used for second harmonic generation. This method is called *critical phase matching*.

A birefringent crystal is one in which the refractive index depends upon the direction of polarization of the propagating light wave. Birefringent crystals are classified based on their atomic geometry as either biaxial or uniaxial [**2**]. Isotropic crystals have a uniform refractive index that is independent of polarization direction, and thus are not defined to be birefringent. For uniaxial crystals there is one principle axis, called the *extraordinary axis*, along which the refractive index is distinct from the other two principle axes (in biaxial crystals all three principle axes have distinct refractive indices). The extraordinary axis in uniaxial crystals is also known as the optic axis, and will be referred to as such for the remainder of this thesis. All polarizations perpendicular to the optic axis experience the same refractive index n_o. Polarizations parallel

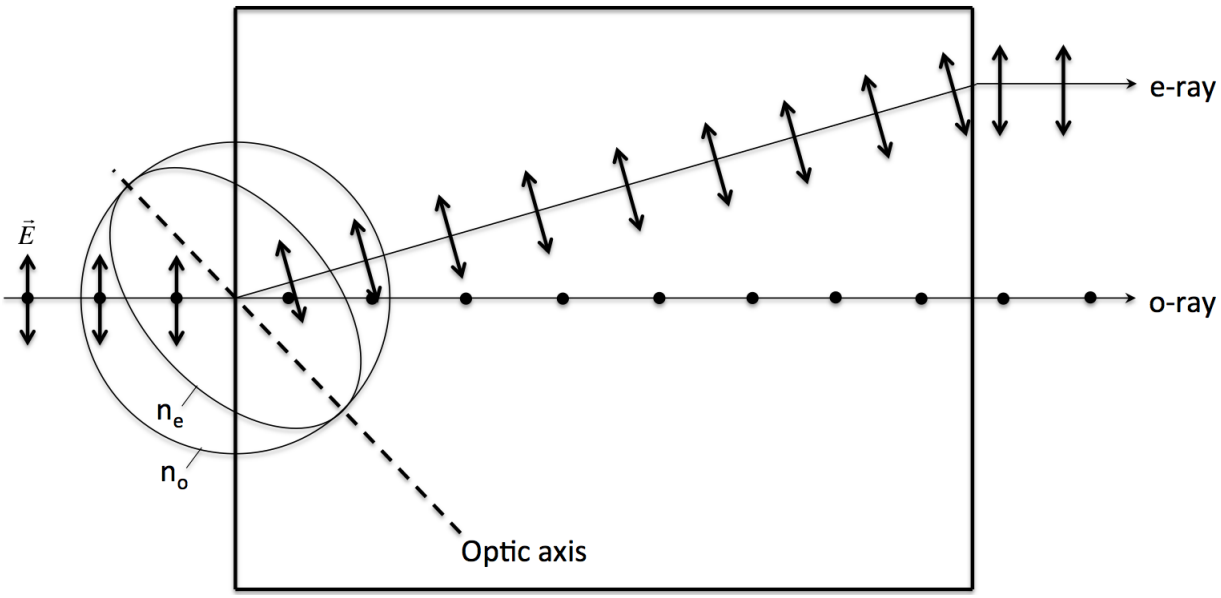

FIGURE 4.1. A light beam with two orthogonal field components traversing a negative uniaxial crystal. The ordinary ray experiences a refractive index $n_o(\omega)$ and the extraordinary ray experiences a refractive index $n_e(\omega, \theta)$.

to the optic axis experience a refractive index n_e. It should be emphasized that the optic axis is a direction and not merely a single line.

Two types of waves can propagate in a birefringent uniaxial crystal, namely, waves plane-polarized perpendicular to the plane formed by the optic axis and the direction of propagation (ordinary waves) which experience a refractive index $n_o(\omega)$, and waves plane-polarized parallel to this plane (extraordinary waves) which experience a refractive index $n_e(\omega, \theta)$ a function of ω and the angle θ between the wavevector $\vec{k}$ and the optic axis. As depicted in Figure 4.1, the o-ray and e-ray experience different indices of refraction. The e-ray is refracted from the normal line (disobeying Snell's law). The angle between the e-ray and o-ray is known as the *walk-off angle*, and will be discussed in the following section.

As given in [**15**] these indices are related by

$$\frac{1}{n_e^2(\omega,\theta)} = \frac{\cos^2\theta}{n_o^2(\omega)} + \frac{\sin^2\theta}{n_e^2(\omega)} \tag{4.6}$$

where $n_e(\omega) = n_e(\omega, \theta = \pi/2)$. Since $\vec{E}$ (whose direction defines the polarization direction of the wave) and $\vec{k}$ are perpendicular, then when $\vec{k}$ is parallel to the optic axis ($\theta = 0$) the polarization will be perpendicular to the optic axis. Since all polarizations perpendicular to the optic axis experience a refractive index $n_o(\omega)$ then we expect (and (4.6) confirms) that $n_e(\omega, 0) = n_o(\omega)$.

One way to achieve the phase matching condition (4.5) is by sending in the fundamental wave as an extraordinary wave propagating at an angle θ_p to the optic axis such that

$$n_e(\omega, \theta_p) = n_o(2\omega). \tag{4.7}$$

This type of second harmonic generation is called e-e-o because on the quantum scale pairs of identical extraordinary photons combine to form one ordinary photon with twice the energy (and frequency) of the first two. The second harmonic wave is generated as an ordinary wave

propagating in the direction θ_p because this is the only direction and polarization for which there is phase matching and thus appreciable second harmonic generation.

Using (4.7) in (4.6) gives

$$\frac{1}{n_o^2(2\omega)} = \frac{1}{n_e^2(\omega,\theta_p)} = \frac{\cos^2\theta_p}{n_o^2(\omega)} + \frac{\sin^2\theta_p}{n_e^2(\omega)}. \tag{4.8}$$

Solving for $\sin^2\theta_p$ we have

$$\sin^2\theta_p = \frac{n_o(\omega)^{-2} - n_o(2\omega)^{-2}}{n_o(\omega)^{-2} - n_e(\omega)^{-2}} \tag{4.9}$$

Assuming that the crystal is normally despersive, $n_o(2\omega) > n_o(\omega)$ and therefore $n_o(\omega)^{-2} - n_o(2\omega)^{-2} > 0$. Thus, in order for $\sin^2\theta_p > 0$ we must have $n_o(\omega)^{-2} - n_e(\omega)^{-2} > 0$ or $n_e(\omega) > n_o(\omega)$. Furthermore, for $\sin^2\theta_p > 0$ we require

$$n_o(\omega)^{-2} - n_e(\omega)^{-2} > n_o(\omega)^{-2} - n_o(2\omega)^{-2} \tag{4.10}$$

or

$$n_e(\omega) > n_o(2\omega). \tag{4.11}$$

Crystals with the property $n_e(\omega) > n_o(\omega)$ are called *positive uniaxial*.

Our experimental setup uses a barium borate BaB_2O_4 (BBO) crystal, which is a birefringent uniaxial crystal for which $n_o(\omega) > n_e(\omega)$. Such a crystal is called *negative uniaxial*. As we have just shown, sending in the fundamental wave as an extraordinary wave at an angle θ_p which satisfies (4.7) will not work for the case of a negative uniaxial crystal. Instead, the fundamental wave is sent in as an ordinary wave propagating at an angle θ_p such that

$$n_o(\omega) = n_e(2\omega,\theta_p), \tag{4.12}$$

satisfying the phase matching condition for efficient second harmonic generation in the θ_p direction. This type of second harmonic generation is called o-o-e because pairs of ordinary photons combine to form extraordinary photons with double the frequency. Since the second harmonic propagates parallel to the fundamental, both the fundamental and extraordinary waves will propagate at θ_p to the optic axis. A similar analysis as before gives

$$\sin^2\theta_p = \frac{n_o(\omega)^{-2} - n_o(2\omega)^{-2}}{n_e(2\omega)^{-2} - n_o(2\omega)^{-2}} \tag{4.13}$$

which requires

$$n_e(2\omega) < n_o(\omega) \tag{4.14}$$

along with $n_o(\omega) > n_e(\omega)$ for the critical phase matching angle θ_p to exist.

Our fundamental beam has wavelength $\lambda = 800\text{nm}$ or $\omega = 2\pi c/\lambda = 2.36 \times 10^{15}\text{Hz}$. According to [**16**] the ordinary and extraordinary indices of refraction of BBO are closely fit by the expressions

$$n_o^2(\lambda) = 2.7359 + \frac{0.01878}{\lambda^2 - 0.01822} - 0.01354\lambda^2$$
$$n_e^2(\lambda) = 2.3753 + \frac{0.01224}{\lambda^2 - 0.01667} - 0.01516\lambda^2$$

for λ given in μm. Using $\lambda_1 = 800$nm and $\lambda_2 = 400$nm in the above expressions gives

$$n_o(\omega) = 1.6606$$
$$n_o(2\omega) = 1.6930$$
$$n_e(2\omega) = 1.5679$$

and using these numbers in (4.13) gives

$$\theta_p = 29.18^\circ \tag{4.15}$$

for the critical phase matching angle.

The critical phase matching angle θ_p is not to be confused with Brewster's angle θ_B, although both are used for SHG optimization. Brewster's angle is one way to eliminate any reflection at the first face of the crystal, which would cause unwanted reduction of the transmitted power and interference of the pump beam with itself. Another way is to anti-reflection (AR) coat the crystal at the fundamental wavelength. Our BBO crystal is AR coated for 800nm and 400nm to be sure that no fundamental or second harmonic light reflects off the surface. As such, we do not need to send in the fundamental at Brewster's angle. However, the topic is an interesting one which can deepen our understanding of the geometry of uniaxial crystals, so I will discuss it briefly for the remainder of this section.

If we view the atomic structure along a principal axis of the crystal as a collection of electric dipoles, then Brewster's angle is the angle of incidence at which the reflected ray aligns parallel to the dipole moment $\vec{p}$ of the interatomic dipoles. Since dipoles cannot produce electromagnetic radiation parallel to $\vec{p}$, the amplitude of the reflected ray goes to zero at Brewster's angle. We also require that θ_B be the angle of incidence at which the transmitted field is maximized. This means the angle between the wavevector of the transmitted field and the dipole moment of the interatomic dipoles must be 90°.

The dotted line in Figure 4.2 represents the axis of the interatomic atomic dipole moments. Note that only components of the optical wave which are plane-polarized parallel to the plane of incidence will be affected by changes in θ_i. Therefore, only the reflected ray of the parallel component will be minimized at Brewster's angle θ_B. Brewster's angle is also referred to as the "polarizing angle" because the reflected ray will be polarized perpendicular to the plane of incidence. Brewster's angle is achieved when $\theta = 0$ or, using the geometry of Figure 4.2, $\theta_r + \theta_t = 90^\circ$. At Brewster's angle we have $\theta_B = \theta_i = \theta_r$, which implies $\theta_B + \theta_t = 90^\circ$.

Snell's law dictates

$$n_i \sin\theta_B = n_t \sin\theta_t. \tag{4.16}$$

Using $\theta_B = 90^\circ - \theta_t$ it follows that

$$n_i \sin\theta_B = n_t \cos\theta_B. \tag{4.17}$$

So Brewster's angle is given by

$$\tan\theta_B = \frac{n_i}{n_t}. \tag{4.18}$$

In practice, the fundamental is sent in as an ordinary wave, which means it is plane-polarized perpendicular to the plane formed by the optic axis and the propagation direction (which form an angle θ_p). Since Brewster's angle lies on the plane formed by the propagation direction and the fundamental beam's polarization direction then the critical phase matching angle θ_p and Brewster's angle θ_B lie on perpendicular planes, as shown in Figure 4.3.

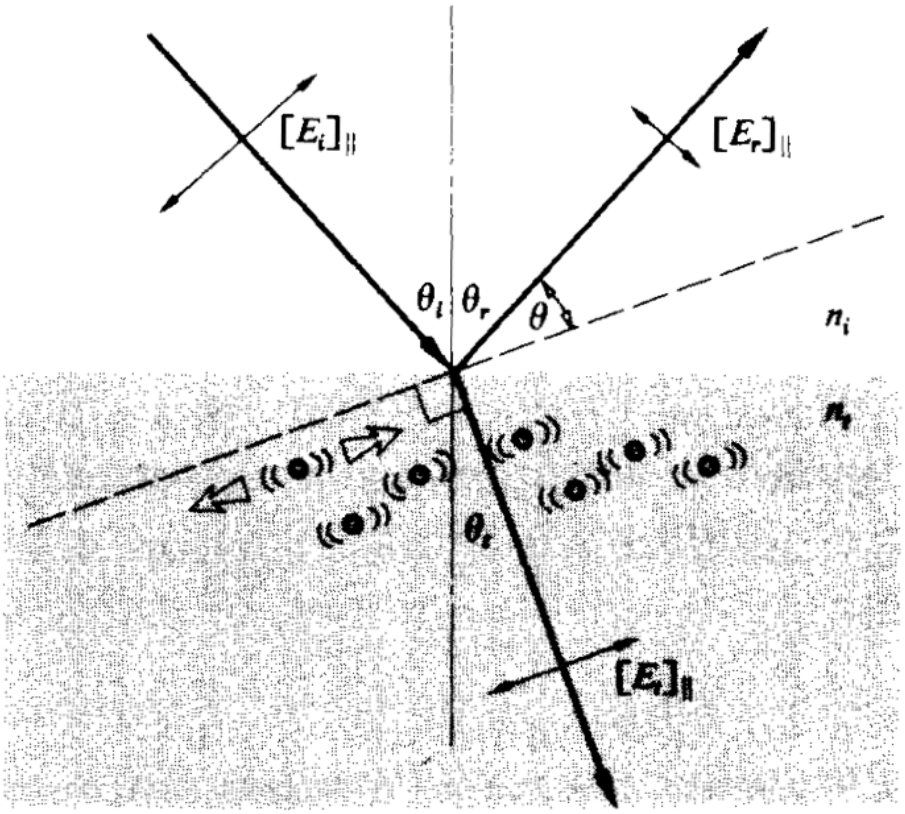

FIGURE 4.2. Interatomic dipole moments and Brewster's angle [**3**].

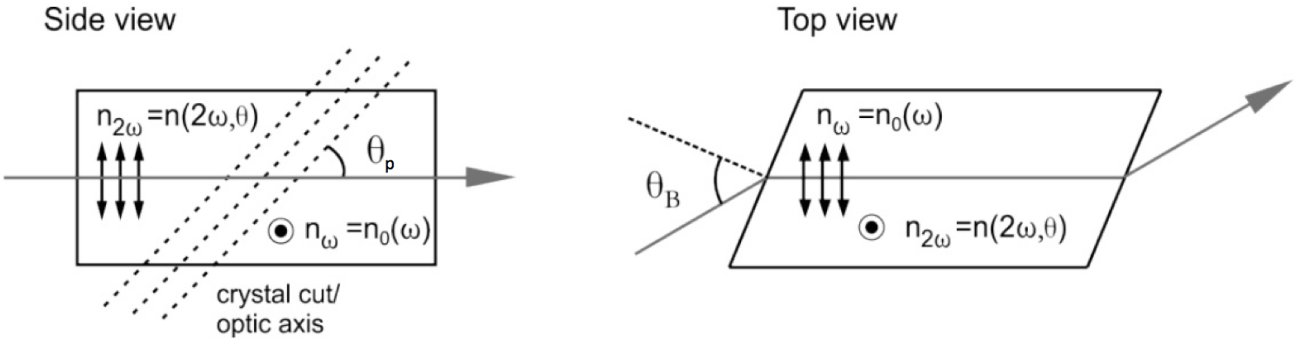

FIGURE 4.3. Type I o-o-e critical phase matching in a negative uniaxial crystal cut at the phase matching angle θ_p and with faces cut at Brewster's angle θ_B [**4**].

2. Walk-Off Angle

This treatment gives frequent reference to [**17**] and [**18**]. If the electric field of the extraordinary wave is not parallel to the optic axis ($\theta_p \neq 0$) then its Poynting vector $\vec{S}$ is not parallel to its wavevector $\vec{k}$. The angle between $\vec{S}$ and $\vec{k}$ is called the *walk-off angle* and is denoted ρ. This angle is equivalent to the angle between the Poynting vectors of the ordinary and extraordinary rays (see Figure 4.1).

To develop a qualitative understanding of this effect we consider an electric field $\vec{E}$ incident on a birefringent negative uniaxial crystal at some non-zero angle relative to the optic axis. By

definition of negative uniaxial $n_o(\omega) > n_e(\omega)$. The component of $\vec{E}$ which is parallel to the optic axis will experience a refractive index $n_e(\omega)$ and will propagate with velocity $v_\parallel = c/n_e$. The component perpendicular to the optic axis will propagate with velocity $v_\perp = c/n_o$. Since $n_o(\omega) > n_e(\omega)$ then $v_\perp < v_\parallel$. Based on this reasoning, we predict the Huygens wavelets for the e-wave will be ellipsoids of revolution about the optic axis, as depicted in Figure 4.4 [**3**].

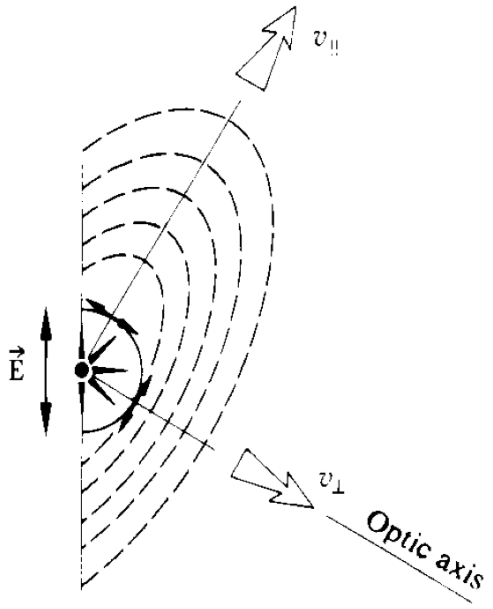

FIGURE 4.4. Ellipsoidal wavelets of e-wave in a negative uniaxial crystal [**3**].

The envelope of infinitessimal ellipsoidal wavelets will create a plane wave propagating in the same direction as the incident wave. Evidently, the ellipsoidal wavelets will also produce a sideways displacement of the plane wave as it propagates through the crystal. While the wavevector $\vec{k}$ follows the same path as before, the direction of energy propagation (the direction of $\vec{S}$) now has a sideways displacement. This phenomenon only occurs for the extraordinary wave, as the ordinary wave is by definition polarized perpendicular to the optic axis, and thus experiences only one refractive index $n_o(\omega)$.

Now we derive an expression for the walk-off angle ρ. Since $\vec{k} \propto \vec{D} \times \vec{B}$ and $\vec{S} \propto \vec{E} \times \vec{B}$ then $\vec{k_e} \perp \vec{D_e}$ and $\vec{S_e} \perp \vec{E_e}$, which implies that ρ is also the angle between $\vec{E}$ and $\vec{D}$. Note that $\vec{D}_e, \vec{E}_e, \vec{S}_e$ and $\vec{k}_e$ all lie in a plane perpendicular to $\vec{B}_e$. We assume that the wave is propagating at the critical angle θ_p from the optic axis. From the geometry of Figure 4.6 we have

$$\vec{D}_e \cdot \vec{E}_e = |\vec{D}_e||\vec{E}_e| \cos\rho. \tag{4.19}$$

We can relate $\vec{D}_e$ and $\vec{E}_e$ through their projections onto the principal axes:

$$D_z^e = n_e^2 \epsilon_0 E_z^e \tag{4.20}$$

and

$$D_{xy}^e = n_o^2 \epsilon_0 E_{xy}^e \tag{4.21}$$

where we have used $n^2 = \epsilon/\epsilon_0$, and assumed the optic axis is in the z-direction. Since the components of $\vec{E}$ in the x and y directions will both experience a refractive index $n_o(\omega)$ we

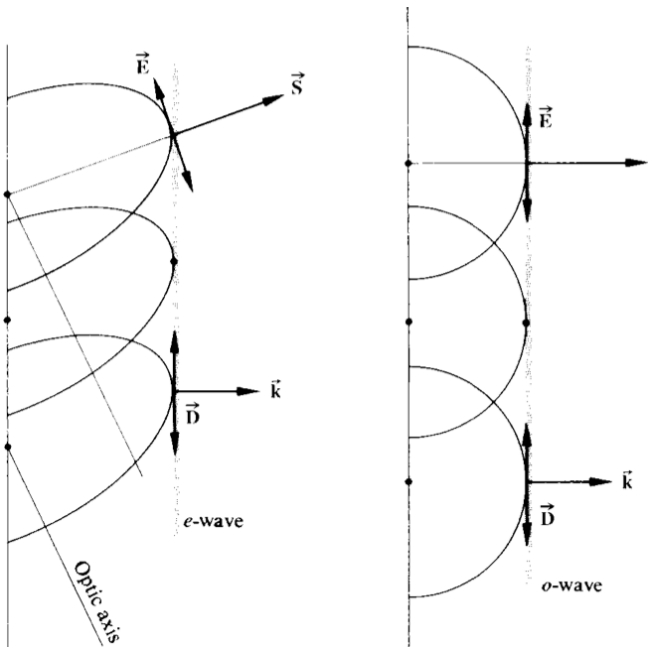

FIGURE 4.5. Orientations of the $\vec{E}, \vec{S}, \vec{D}$, and $\vec{k}$ vectors for ordinary and extra-ordinary wavelets [**3**].

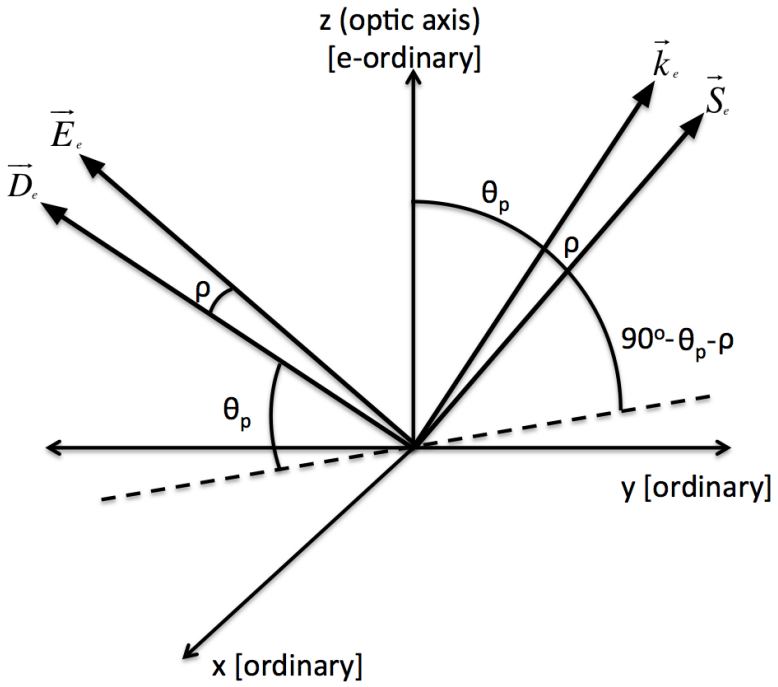

FIGURE 4.6. Walk-off angle.

have made the problem two-dimensional by projecting $\vec{E}$ onto the xy-plane (we will refer to this plane later as the *ordinary plane*.

The expressions (4.20) and (4.21) are valid only in the limit of a linear polarization given by $\vec{P} = \epsilon_0 \chi^{(1)} \vec{E}$. We return to a linear approximation of $\vec{P}$ because it simplifies the analysis significantly with minimal loss of accuracy.

Writing $\vec{D}$ as a sum of projections onto the principal axes:

$$\vec{D}_e \cdot \vec{E}_e = E^e_{xy} D^e_{xy} + E^e_z D^e_z. \tag{4.22}$$

Using the geometry of Figure 4.6 we have

$$\begin{aligned} D^e_{xy} &= D \cos\theta_p \\ D^e_z &= D \sin\theta_p. \end{aligned}$$

Using these expressions, (4.20), (4.21), and (4.22) in (4.19) gives

$$\cos\rho = \frac{\vec{D}_e \cdot \vec{E}_e}{|\vec{D}_e||\vec{E}_e|} \tag{4.23}$$

$$= \frac{D^e_{xy} E^e_{xy} + D^e_z E^e_z}{\left[(D^e_{xy})^2 + (D^e_z)^2\right]^{1/2} \left[(E^e_{xy})^2 + (E^e_z)^2\right]^{1/2}} \tag{4.24}$$

$$= \frac{D_e^2 \left[\frac{\cos^2\theta_p}{n_o^2} + \frac{\sin^2\theta_p}{n_e^2}\right]}{D_e^2 \left[\frac{\cos^2\theta_p}{n_o^4} + \frac{\sin^2\theta_p}{n_e^4}\right]^{1/2}} \tag{4.25}$$

which implies

$$\cos^2\rho = \frac{\left[\frac{\cos^2\theta_p}{n_o^2} + \frac{\sin^2\theta_p}{n_e^2}\right]^2}{\left[\frac{\cos^2\theta_p}{n_o^4} + \frac{\sin^2\theta_p}{n_e^4}\right]}. \tag{4.26}$$

Using the identity

$$\tan^2\rho = \frac{1}{\cos^2\rho} - 1 \tag{4.27}$$

(4.26) simplifies to

$$\tan\rho = \frac{1}{2}\left[\frac{\cos^2\theta_p}{n_o^2} + \frac{\sin^2\theta_p}{n_e^2}\right]^{-1} \left(\frac{1}{n_e^2} - \frac{1}{n_o^2}\right) \sin 2\theta_p. \tag{4.28}$$

Employing (4.6) and (4.12) we find that the walk-off angle for the second-harmonic in negative uniaxial crystals is given by

$$\rho = \arctan\left(\frac{1}{2} n_o^2(\omega) \sin 2\theta_p \left[n_e^{-2}(2\omega) - n_o^{-2}(2\omega)\right]\right). \tag{4.29}$$

Using the values of θ_p, $n_o(\omega)$, $n_o(2\omega)$ and $n_e(2\omega)$ given previously and in a table at the end of this thesis, for second harmonic generation of 800nm light in a BBO crystal we find

$$\rho = 3.89^\circ. \tag{4.30}$$

This result will be used in the following section to optimize second harmonic generation.

3. Focused Gaussian Beam SHG Optimization

The theory of second harmonic generation with focused Gaussian beams has been developed in detail by Boyd and Kleinman [**19**]. They derive the optimal focal properties of the fundamental beam given the crystal length, walk-off angle, and refractive indices of the medium. They find the optimal beam properties for given values of the so-called *walk-off parameter* B which is given by

$$B = \frac{1}{2}\rho\sqrt{lk^{(\omega)}} \tag{4.31}$$

where $k^{(\omega)}$ is the wavenumber corresponding to the fundamental wave. For second harmonic generation with a birefringent negative uniaxial crystal we will have $k^{(\omega)} = \omega n_o(\omega)/c$. The optimal focal properties as a function of B become asymptotic for $B > 6$, so it is desirable to meet this condition. We use a BBO crystal of length $l = 9$mm, which gives $B \cong 18$.

Boyd and Kleinman find when $B > 6$ second harmonic generation is maximized when

$$\frac{l}{2z_0} = 1.39 \tag{4.32}$$

where $z_0 = \pi w_0^2/\lambda$ is the Rayleigh range of the focused Gaussian beam. Solving for w_0 we find the optimum beam waist is given by

$$w_0 = \sqrt{\frac{\lambda l}{2.78\pi}}. \tag{4.33}$$

In our case $\lambda = 800$nm and $l = 9$mm so the optimal beam waist is

$$w_0 = 2.87 \times 10^{-5}\text{m}. \tag{4.34}$$

The angular divergence of a Gaussian beam is approximated by (1.42) as

$$\theta = \frac{\lambda}{\pi w_0}. \tag{4.35}$$

If we assume the beam begins perfectly collimated with diameter D and then is focused by an optical element of focal length F such that w_0 lies in the center of the crystal then we can also approximate θ by

$$\theta = \frac{D/2}{F}. \tag{4.36}$$

Combining these expressions we find the optimal optical focal length F to be

$$F = \frac{w_0\pi D}{2\lambda}. \tag{4.37}$$

We use a Ti:Sapphire laser with diameter $D = 2$mm. Using $\lambda = 800$nm and $w_0 = 2.87 \times 10^{-5}$m we find

$$F = 11.3\text{cm} \tag{4.38}$$

for optimal second harmonic generation.

With the optimal beam characteristics in hand we can now calculate a predicted conversion efficiency with (3.70). Since BBO is a negative uniaxial crystal the pump beam will be an ordinary ray and the second harmonic will be an extraordinary ray. Thus, we use $n_0(\omega)$ and $n_e(2\omega)$ in (3.70). Further, the permeability of optical materials such as BBO is close enough to that of free space that we may substitute μ_0 for μ. BBO has a nonlinear coefficient of

approximately $d = 1.95 \times 10^{-23}$ for extraordinary rays. Our crystal length is 9mm. For an input power of 100mW (3.70) gives

$$\eta_{\text{SHG}} = 0.00016 \tag{4.39}$$

which is a conversion efficiency of 0.016% and corresponds to an expected SHG output power of 16μW for single pass.

4. Resonant Enhancement Cavity

To further increase the second-harmonic light generated the nonlinear crystal is placed in a cavity of two or more mirrors which facilitate many passes of the pump beam through the crystal. If the pump beam is resonant with the cavity and properly mode matched to it the resulting circulating power is far greater than the incident power.

Most resonant cavities have a bowtie configuration, as shown in Figure 4.7. All mirrors are highly reflective at the pump beam frequency, except for M1 which is slightly transmissive to allow the fundamental wave to enter the cavity. All mirrors are also anti-reflective at the second harmonic frequency.

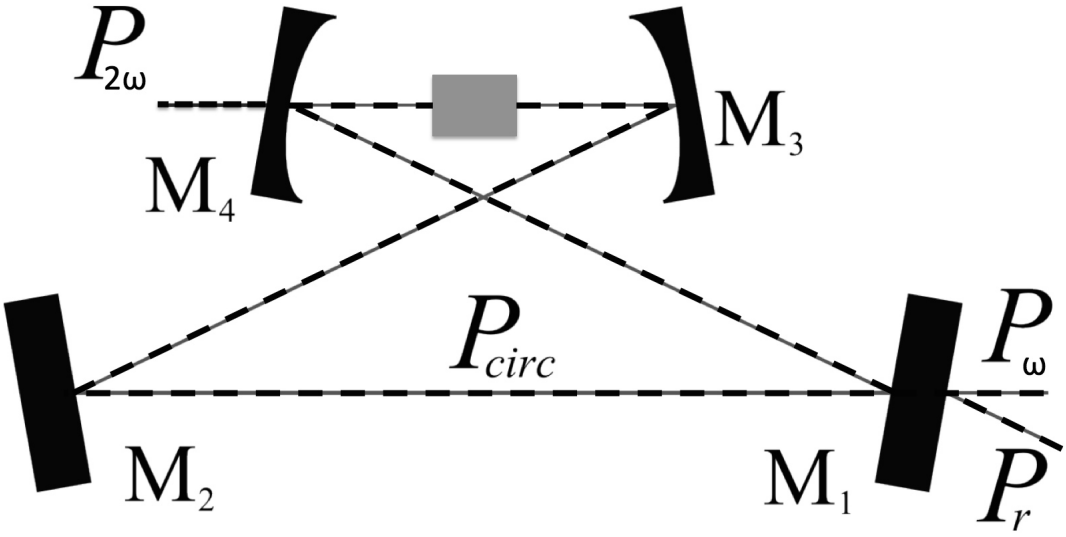

FIGURE 4.7. Bowtie cavity for resonant enhancement of the input fundamental wave [**5**].

The circulating fundamental beam must constructively interfere with the continuous beam of fundamental light transmitted through M1. Thus, the *complex beam parameter* given by

$$q(z) = \left(\frac{1}{R(z)} - i \frac{\lambda}{\pi \omega^2(z)} \right)^{-1} \tag{4.40}$$

must be reproduced after one round trip through the cavity. This condition can be achieved by proper choice of cavity geometry and mirror radii of curvature. Softwares such as Winlase are available to calculate $q(z)$ at all points in an optical system for a given set of initial parameters [**5**].

5. Cavity Stabilization

The cavity must be stabilized so that it is always resonant with the fundamental ordinary ray. Mechanical vibrations and temperature changes cause both the cavity length and the laser phase to drift from resonance. One widely used locking scheme was proposed by Hänsch and Couillaud (HC) [**6**]. This technique is unique in that it does not require active frequency modulation of the laser to provide active feedback to the cavity. Methods such as the Pound-Drever-Hall scheme which use active frequency modulation are more stable but much more expensive.

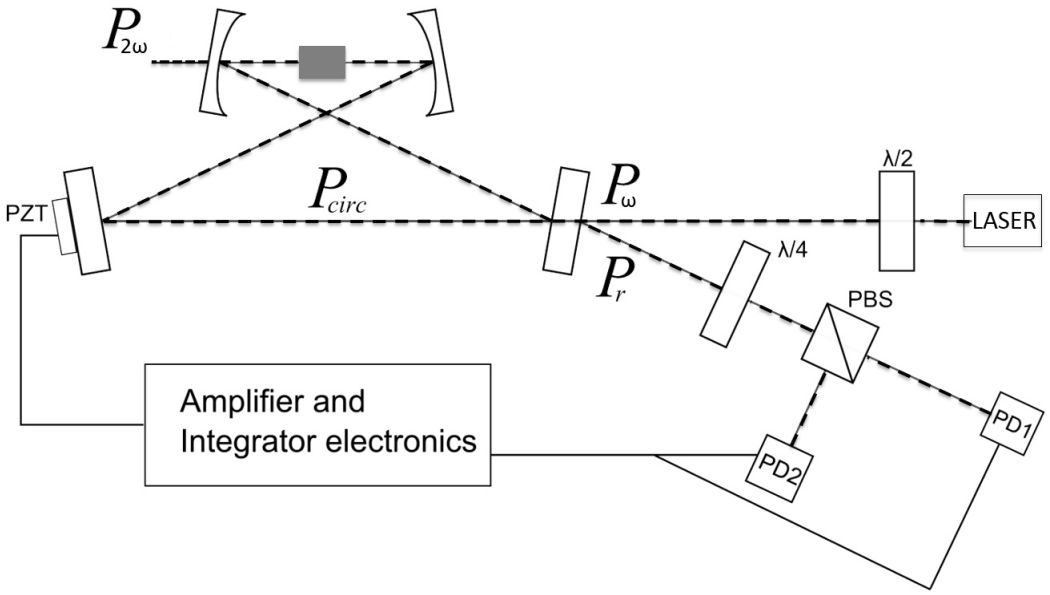

FIGURE 4.8. Hänsch-Couillaud cavity locking scheme [**5**].

First harmonic light is incident on the resonant cavity with power P_ω. The $\lambda/2$ waveplate is used to align the polarization to a small angle θ (usually $\sim 5°$) with respect to the ordinary plane (the xy-plane in Figure 4.6) of the birefringent crystal. The incident beam's electric field can be decomposed into components parallel and perpendicular to the ordinary plane of the crystal:

$$E^i_\parallel = E^i \cos\theta \tag{4.41}$$

$$E^i_\perp = E^i \sin\theta \tag{4.42}$$

The parallel component propagates as an ordinary wave. The cavity is optimized to be resonant with the ordinary wave, so the parallel component experiences a low-loss cavity. Thus, the reflected ray at M1 will have a parallel component which includes the initial reflection at M1 as well as an infinite sum of electromagnetic waves built up in the cavity and transmitted back through M1. Using the standard approach [**15**] the parallel component of the reflected ray can be calculated as

$$E^r_\parallel = E^i_\parallel \left[\sqrt{R_1} - \frac{T_1}{\sqrt{R_1}} \frac{Re^{i\delta}}{1 - Re^{i\delta}} \right] \tag{4.43}$$

$$= E^i_\parallel \left[\sqrt{R_1} - \frac{T_1 R}{\sqrt{R_1}} \frac{\cos\delta - R + i\sin\delta}{(1-R)^2 + 4R\sin^2(\delta/2)} \right]. \tag{4.44}$$

where δ is the phase accumulated by the wave as it propagates through the cavity, R_1 and T_1 are the reflectivity and transmittivity of M1 and $R < 1$ gives the amplitude ratio between successive round trips, which determines the cavity finesse $\mathscr{F} = \pi\sqrt{R}/(1-R)$. The ratio R accounts for any attenuation by the crystal and any other losses in the cavity.

The perpendicular component is extraordinary, and so is not resonant with the cavity. Thus, the perpendicular component of the reflected ray is to first approximation

$$E_\perp^r = E_\perp^i \sqrt{R_1}. \tag{4.45}$$

At exact resonance ($\delta = 2n\pi$) both reflected components are real and in phase. Off resonance the parallel component acquires a nonzero imaginary term and the recombined beam becomes elliptically polarized. The magnitude of the ellipticity of the reflected ray is therefore a measure of the detuning from resonance. Moreover, the handedness depends on the sign of the detuning.

The lower right portion of the experimental setup depicted in Figure 4.8 is for analyzing the polarization of the reflected wave. The $\lambda/4$ waveplate is used to align the reflected wave at 45° to the polarization axis of the polarizing beam splitter output a. The intensities of the two polarizations are measured using the two photodiodes PD1 and PD2, whose outputs are fed to a differential amplifier. The signal from the differential amplifier is given by the function [**6**]

$$I_a - I_b = 2I^i \cos\theta \sin\theta \frac{T_1 R \sin\delta}{4R(1-R)^2 \sin^2(\delta/2)} \tag{4.46}$$

where $I^i = 1/2c\epsilon|E^i|^2$ is the intensity of the input beam and θ is the angle between the incident polarization and the ordinary plane. Increasing θ results in a better signal to noise ratio through $\cos\theta\sin\theta$, but at the expense of losing some circulating pump power. This function is plotted in Figure 4.9. Note that the slope is negative when far from resonance, and positive when very close to resonance. This opens the possibility for automatic electronic relocking to resonance. Interestingly, this error signal may either be fed to an internal laser piezo to lock its frequency to the cavity (Figure 4.10), or it may be fed to a piezo placed on one of the cavity mirrors to lock the cavity to be resonant with the laser frequency (Figure 4.8).

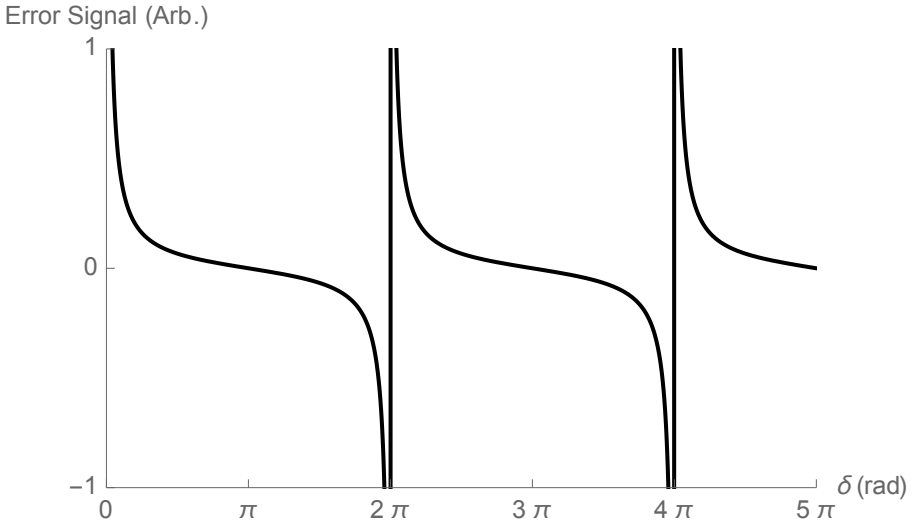

FIGURE 4.9. Plot of error signal (4.46) as function of detuning from resonance in Hänsch-Couillaud locking scheme.

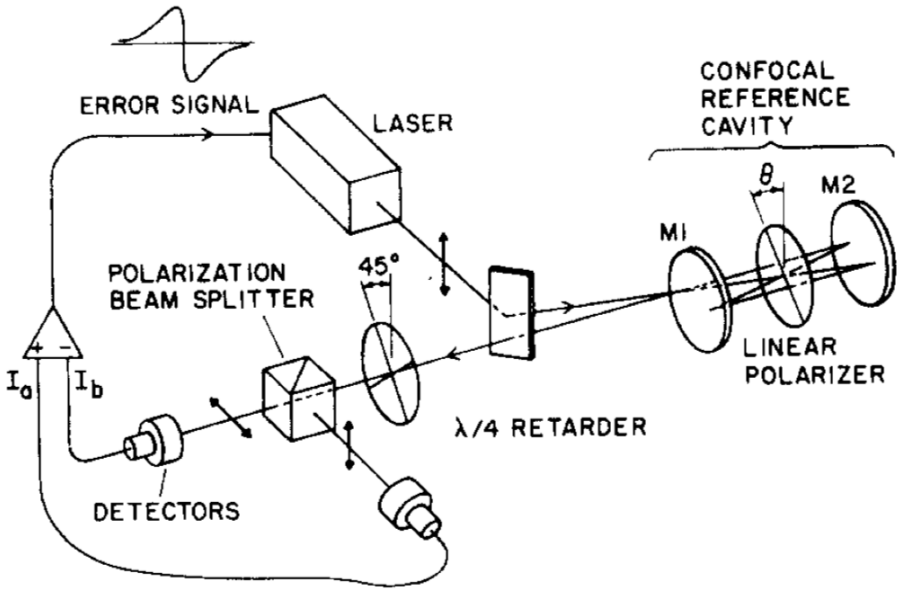

FIGURE 4.10. Hänsch-Couillaud locking scheme used to lock the laser frequency to be resonant with a cavity [**6**].

$\lambda_1 = 800\text{nm}$	Fundamental wavelength
$\lambda_2 = 400\text{nm}$	Second harmonic wavelength
$D = 2\text{mm}$	Ti:Sapphire laser beam diameter
$n_o(\omega) = 1.6606$	Ordinary refractive index at fundamental frequency
$n_o(2\omega) = 1.6930$	Ordinary refractive index at second harmonic frequency
$n_e(2\omega) = 1.5679$	Extraordinary refractive index at second harmonic frequency
$F = 11.3\text{cm}$	Optimal focal length of focusing element
$w_0 = 2.87 \times 10^{-5}\text{m}$	Optimal beam waist for SHG
$\theta_p = 29.18°$	Optimal critical phase-matching angle

TABLE 1. Relevant values for optimal second harmonic generation with given input beam characteristics.

Material	BBO Crystal
Dimensions	$(3x3 \pm 0.1)$mm
Thickness	9mm
Surface Quality	10-5, scratch-dig
Flatness	Lambda/6 at 633 nm
Parallelism	< 5 arcminutes
Other faces	Fine grind
Coating	AR/AR at 800nm and 400nm
Phase-matching angle	29.2°

TABLE 2. Crystal Specifications.

Appendix

Intensity of Monochomatic Plane Waves

Here we derive an expression for the intensity of monochromatic plane waves:

$$I = \frac{1}{2}\sqrt{\frac{\epsilon_0}{\mu_0}}|E_0(z)|^2. \tag{4.49}$$

It is straightforward to derive the work needed to assemble a static charge distribution against the Coulomb force between charges [**20**]:

$$W_e = \frac{\epsilon_0}{2}\int\limits_{\text{all space}} E^2 d\tau \tag{4.50}$$

where $d\tau$ is an infinitessimal volume element and $\vec{E}$ is the resulting electric field.

Likewise, the work required to get currents going against the back emf is

$$W_m = \frac{1}{2\mu_0}\int\limits_{\text{all space}} B^2 d\tau \tag{4.51}$$

where $\vec{B}$ is the resulting magnetic field. Since electromagnetic fields consist exclusively of moving and stationary charges, this implies that the total energy stored in electromagnetic fields per unit volume is

$$u = \frac{1}{2}\left(\epsilon_0 E^2 + \frac{1}{\mu_0}B^2\right). \tag{4.52}$$

We are interested in a monochromatic plane wave traveling in the $\hat{z}$ direction. The electric and magnetic fields for such a wave are given by

$$\vec{E}(z,t) = E_0(z)\cos(kz - \omega t + \delta)\hat{x} \tag{4.53}$$

$$\vec{B}(z,t) = \frac{1}{c}E_0(z)\cos(kz - \omega t + \delta)\hat{y} \tag{4.54}$$

which implies

$$B^2 = \frac{1}{c^2}E^2 = \mu_0\epsilon_0 E^2. \tag{4.55}$$

Using (4.55) in (4.52) gives

$$u = \frac{1}{2}\left(\epsilon_0 E^2 + \frac{1}{\mu_0}B^2\right) = \frac{1}{2}\left(\epsilon_0 E^2 + \epsilon_0 E^2\right) = \epsilon_0 E^2 = \epsilon_0|E_0|^2\cos^2(kz - \omega t + \delta). \tag{4.56}$$

Interestingly, the contributions to the energy stored per unit volume u from the electric and magnetic fields are equal.

The energy flux density (energy per unit area, per unit time) transported by the fields is given by the Poynting vector

$$\vec{S} = \frac{1}{\mu_0}(\vec{E} \times \vec{B}). \tag{4.57}$$

For a monochromatic plane wave traveling in the z-direction,

$$\vec{S} = c\epsilon_0 |E_0|^2 \cos^2(kz - \omega t + \delta)\hat{z} = cu\hat{z}. \tag{4.58}$$

The relation $\vec{S} = cu\hat{z}$ can also be derived by considering that in a time Δt a length $c\Delta t$ of the electromagnetic wave passes through an area A carrying with it an energy $u * (\text{Volume}) = u(Ac\Delta t)$. The energy per unit time, per unit area, transported by the wave is thus uc.

The *intensity* of the wave is defined as the (time) average power per unit area transported by an electromagnetic wave:

$$I \equiv < S >= \frac{1}{T} c\epsilon_0 |E_0|^2 \int_0^T \cos^2(kz - \omega t + \delta) dt \tag{4.59}$$

where T denotes one period of oscillation. Evaluating (4.59) gives

$$I = \frac{1}{2} c\epsilon_0 |E_0(z)|^2 \tag{4.60}$$

or

$$I = \frac{1}{2}\sqrt{\frac{\epsilon_0}{\mu_0}} |E_0(z)|^2. \tag{4.61}$$

Bibliography

[1] Jody Muelaner. Laser interferometers. http://www.muelaner.com/laser-interferometers/. Accessed: 2015-03-16.

[2] R.W. Boyd. *Nonlinear Optics*. Elsevier Science, 2013.

[3] E. Hecht. *Optics*. Addison-Wesley, 2002.

[4] Radu Mircea Cazan. Preparation of cold mg+ ion clouds for sympathetic cooling of highly charged ions at spectrap. Johannes Gutenberg University Ph.D Thesis.

[5] Ian Norris. Laser cooling and trapping of neutral calcium atoms. University of Strathclyde Ph.D Thesis.

[6] T. W. Hansch and B. Couillaud. Laser frequency stabilization by polarization spectroscopy of a reflecting reference cavity. *Optics Communications*, 35(3):441–444, December 1980.

[7] P. A. Franken, A. E. Hill, C. W. Peters, and G. Weinreich. Generation of optical harmonics. *Phys. Rev. Lett.*, 7:118–119, Aug 1961.

[8] N. Bloembergen and P. S. Pershan. Light waves at the boundary of nonlinear media. *Phys. Rev.*, 128:606–622, Oct 1962.

[9] Shumpei Masuda, Katsuhiro Nakamura, and Adolfo del Campo. High-fidelity rapid ground-state loading of an ultracold gas into an optical lattice. *Phys. Rev. Lett.*, 113:063003, Aug 2014.

[10] P.W. Milonni and J.H. Eberly. *Lasers*. Wiley Series in Pure and Applied Optics. Wiley, 1988.

[11] P.F. Goldsmith. *Quasioptical Systems: Gaussian Beam Quasioptical Propogation and Applications*. IEEE Press Series on RF and Microwave Technology. Wiley, 1998.

[12] A. Yariv. *Optical Electronics in Modern Communications*. Number v. 1 in The Oxford series in electrical and computer engineering. Oxford University Press, 1997.

[13] G.C. Baldwin. *An Introduction to Nonlinear Optics*. Plenum Press, 1969.

[14] B.E.A. Saleh and M.C. Teich. *Fundamentals of photonics*. Wiley series in pure and applied optics. Wiley, 1991.

[15] M. Born, E. Wolf, and A.B. Bhatia. *Principles of Optics: Electromagnetic Theory of Propagation, Interference and Diffraction of Light*. Cambridge University Press, 1999.

[16] Institute of Photonics and Electronics. Second Harmonic Generation in a BBO Crystal nonlinear optics tutorial 8. https://ihq.webarchiv.kit.edu/studies/NLO/downloads/SS2011/NLO_SS2011_Tut8_Solution.pdf. Accessed: 2015-03-14.

[17] J. Liu. *Photonic Devices*. Cambridge University Press, 2005.

[18] M. Sheik-Bahae. Homework 2 nonlinear optics (phyc/ece 568). http://www.optics.unm.edu/sbahae/physics568/HW13_2_Solution.pdf. Accessed: 2015-03-15.

[19] G. D. Boyd and D. A. Kleinman. Parametric Interaction of Focused Gaussian Light Beams. *Journal of Applied Physics*, 39:3597–3639, July 1968.

[20] D.J. Griffiths. *Introduction to Electrodynamics*. Always learning. Pearson, 2013.